NAVAL POSTGRADUATE SCHOOL

MONTEREY, CALIFORNIA

THESIS

ACCELERATED NOISE INTERFEROMETRY-BASED PASSIVE ACOUSTIC CHARACTERIZATION OF THE LITTORAL OCEAN

by

Yi-fan Shen

September 2021

Thesis Advisor: Oleg A. Godin
Co-Advisor: Derek Olson

THIS PAGE INTENTIONALLY LEFT BLANK

REPORT DOCUMENTATION PAGE			*Form Approved OMB No. 0704-0188*

1. AGENCY USE ONLY *(Leave blank)*	**2. REPORT DATE** September 2021	**3. REPORT TYPE AND DATES COVERED** Master's thesis

4. TITLE AND SUBTITLE ACCELERATED NOISE INTERFEROMETRY-BASED PASSIVE ACOUSTIC CHARACTERIZATION OF THE LITTORAL OCEAN	**5. FUNDING NUMBERS** RPP11
6. AUTHOR(S) Yi-fan Shen	
7. PERFORMING ORGANIZATION NAME(S) AND ADDRESS(ES) Naval Postgraduate School Monterey, CA 93943-5000	**8. PERFORMING ORGANIZATION REPORT NUMBER**
9. SPONSORING / MONITORING AGENCY NAME(S) AND ADDRESS(ES) Office of Naval Research, Arlington, VA 22203, and National Science Foundation, 2415 Eisenhower Avenue, Alexandria, Virginia 22314	**10. SPONSORING / MONITORING AGENCY REPORT NUMBER**

11. SUPPLEMENTARY NOTES The views expressed in this thesis are those of the author and do not reflect the official policy or position of the Department of Defense or the U.S. Government.

12a. DISTRIBUTION / AVAILABILITY STATEMENT Approved for public release. Distribution is unlimited.	**12b. DISTRIBUTION CODE** A

13. ABSTRACT (maximum 200 words)

Acoustic remote sensing of the ocean traditionally relies on controlled sound sources and active sonars. Alternatively, the seabed and the water column can be characterized acoustically in a surreptitious and environmentally friendly way using noise interferometry. Noise interferometry exploits ambient sound as a signal to probe the environment. Empirical acoustic Green's functions are retrieved from cross-correlations of diffuse noise that is measured concurrently by spatially separated hydrophones. Continuous, multi-day noise-averaging periods were employed in the past to capture noise from numerous noise sources. Long averages achieved maximum diffusivity of ambient sound and retrieved the Green's function with high accuracy required for ocean remote sensing. However, usefulness of the long averaging times is limited by rapid variations in the acoustic propagation environment, e.g., due to internal gravity waves and tides. Using the data acquired in the Shallow Water 2006 experiment on the continental shelf off New Jersey, this thesis focuses on accelerating the noise-interferometry process by judiciously selecting periods where ambient sound is sufficiently diffuse. The goal is to reduce the total time needed for passive acoustic characterization of the seabed and increase the time resolution of acoustic measurements of the water-column properties, thus extending the applications of noise interferometry in naval operations.

14. SUBJECT TERMS noise interferometry, geoacoustic inversion, ambient sound	**15. NUMBER OF PAGES** 67
	16. PRICE CODE

17. SECURITY CLASSIFICATION OF REPORT	**18. SECURITY CLASSIFICATION OF THIS PAGE**	**19. SECURITY CLASSIFICATION OF ABSTRACT**	**20. LIMITATION OF ABSTRACT**
Unclassified	Unclassified	Unclassified	UU

NSN 7540-01-280-5500

Standard Form 298 (Rev. 2-89)
Prescribed by ANSI Std. 239-18

THIS PAGE INTENTIONALLY LEFT BLANK

Approved for public release. Distribution is unlimited.

ACCELERATED NOISE INTERFEROMETRY-BASED PASSIVE ACOUSTIC CHARACTERIZATION OF THE LITTORAL OCEAN

Yi-fan Shen
Lieutenant, Taiwan Navy
BS, Chung Cheng Institute of Technology, National Defense University, 2014

Submitted in partial fulfillment of the
requirements for the degrees of

MASTER OF SCIENCE IN ENGINEERING ACOUSTICS

and

MASTER OF SCIENCE IN PHYSICAL OCEANOGRAPHY

from the

NAVAL POSTGRADUATE SCHOOL
September 2021

Approved by: Oleg A. Godin
Advisor

Derek Olson
Co-Advisor

Oleg A. Godin
Chair, Department of Physics

Peter C. Chu
Chair, Department of Oceanography

THIS PAGE INTENTIONALLY LEFT BLANK

ABSTRACT

Acoustic remote sensing of the ocean traditionally relies on controlled sound sources and active sonars. Alternatively, the seabed and the water column can be characterized acoustically in a surreptitious and environmentally friendly way using noise interferometry. Noise interferometry exploits ambient sound as a signal to probe the environment. Empirical acoustic Green's functions are retrieved from cross-correlations of diffuse noise that is measured concurrently by spatially separated hydrophones. Continuous, multi-day noise-averaging periods were employed in the past to capture noise from numerous noise sources. Long averages achieved maximum diffusivity of ambient sound and retrieved the Green's function with high accuracy required for ocean remote sensing. However, usefulness of the long averaging times is limited by rapid variations in the acoustic propagation environment, e.g., due to internal gravity waves and tides. Using the data acquired in the Shallow Water 2006 experiment on the continental shelf off New Jersey, this thesis focuses on accelerating the noise-interferometry process by judiciously selecting periods where ambient sound is sufficiently diffuse. The goal is to reduce the total time needed for passive acoustic characterization of the seabed and increase the time resolution of acoustic measurements of the water-column properties, thus extending the applications of noise interferometry in naval operations.

THIS PAGE INTENTIONALLY LEFT BLANK

TABLE OF CONTENTS

THIS PAGE INTENTIONALLY LEFT BLANK

LIST OF FIGURES

LIST OF TABLES

THIS PAGE INTENTIONALLY LEFT BLANK

LIST OF ACRONYMS AND ABBREVIATIONS

GF	Green's function
EGF	Empirical Green's function
HLA	horizontal line array
NCCF	noise cross-correlation function
NI	noise interferometry
N-NCCF	negative-time-delay part of the noise cross-correlation function
P-NCCF	positive-time-delay part of the noise cross-correlation function
SHRU	single hydrophone receiving unit
SW06	Shallow Water 2006 Experiment

THIS PAGE INTENTIONALLY LEFT BLANK

ACKNOWLEDGMENTS

I would like to express my deepest appreciation to my advisor, Dr. Oleg Godin, for advising me throughout the research. Without his extensive acoustic knowledge and patient guidance, I would not have been able to complete this thesis. I also would like to thank my co-advisor, Dr. Derek Olson, for his insightful suggestions and constructive help to make this thesis convincing and understandable. Thanks also should go to Dr. Tsu-Wei Tan (R.O.C. Navy) for his invaluable assistance across the Pacific Ocean.

I also would like to extend my gratitude to my USW cohorts, LCDR Darryl Gervis (Canada Navy), MAJ Dexter Tan (Singapore Navy), LT Hwanhee Lee (Korea Navy), ENS Jared Young (U.S. Navy), and other METOC partners, for all the academic support and the lifelong friendship.

Lastly, I am grateful for my beloved wife, Yibei, and my family, who sacrifice a great deal for my dreams. Without them, I would not have been able to overcome these academic challenges.

THIS PAGE INTENTIONALLY LEFT BLANK

I. INTRODUCTION

Understanding the battlefield is strategically important to military operations. Knowledge of the environmental conditions is an integral part of such an understanding in naval planning and operations, especially in the context of undersea warfare. The underwater environment is traditionally characterized using ship-based contact measurements and active sonar systems. However, performing such traditional measures may be problematic in contested areas. Active acoustic methods are usually capital-intensive, power-hungry, and create signals that potentially harm marine animals. Moreover, signals of active sonars are usually apparent in the surrounding background noise and easily detected by the adversary, thus drawing unwanted attention. This is undesirable especially in sensitive waters, such as the Taiwan Strait [1] and the South China Sea [2]. These drawbacks of the traditional ocean sensing means limit their military uses.

This thesis focuses on an alternative, passive approach to remote sensing of the ocean and specifically on acoustic noise interferometry [3]-[5]. Noise interferometry employs ambient underwater sound rather than controlled sound sources to probe the environment. Using this method, one can clandestinely monitor the underwater environment with little power consumption and minimal footprint. Acoustic noise interferometry relies on retrieval of an estimate of the acoustic Green's function, which is usually referred to as the empirical Green's function (EGF), from cross-correlations of the noise records acquired by synchronized, spatially separated receivers [3]-[5]. The Green's function can be viewed as an approximation of the acoustic impulse response of the ocean or as the acoustic field due to a point source and measured at another point. Accurately measured EGF provides as useful information about the environment as can be obtained using a controlled sound source. Successful retrieval of EGF from noise cross-correlation function (NCCF) requires the noise to be sufficiently diffuse, i.e., being generated by multiple, widely spatially distributed noise sources [3]-[6], and can be accurately measured at both hydrophones.

In the underwater context, noise interferometry provides a novel avenue for addressing a variety of applications that usually rely on contact measurements or complex

active sonar systems. For example, Sabra et al. [4] have confirmed the feasibility of array element localization using ambient noise. Noise interferometry has been used to synchronize clocks on distant acoustic receiving systems [4], [7] and measure sound speed profile in deep water [8]. In the Florida Straits Noise Interferometry Experiment, Godin et al. [7] passively measured the flow-induced acoustic nonreciprocity and inverted these measurements to retrieve depth-averaged velocity of the Florida current. Woolfe et al. [9] successfully demonstrated passive acoustic thermometry of the ocean.

On the continental shelf and in other shallow-water environments, dispersion curves of acoustic normal modes, i.e., the dependence of modal group speeds on the sound frequency and the mode order, contain extensive information about the physical properties of the water column and the seabed. Tan et al. [10] have demonstrated that the dispersion curves of low-order normal modes can be successfully retrieved from measured EGFs. In Ref. [6], EGFs were obtained from the NCCFs based on the data acquired during the Shallow Water 2006 Experiment (SW06) on the continental shelf off New Jersey. Time series of noise were recorded continuously on multiple hydrophones during the 15-day observation period from 18 Aug. to 1 Sep. 2006. The employed acoustic data were measured by one of five Single Hydrophone Receiving Units (SHRU) and 32 hydrophones of the Horizontal Line Array (HLA) SHARK. A geoacoustic inversion of the passively measured mode dispersion curves produced a geoacoustic model of the seabed that proved consistent with the results obtained independently using active techniques [6]. The same dataset is used in this thesis. Additionally, using the same HLA but a different SHRU, Mcmullin [11] has found that the quality of NCCFs evaluated using certain one-day observation periods is at least as good as of those obtained using 28 days of data. Despite employing a different SHRU than the one used in this thesis, Mcmullin's results [11] suggest the feasibility of producing EGFs from shorter observation periods.

Passive acoustic measurements of environmental parameters with oceanographically relevant accuracy require precise measurements of EGFs [7]-[10]. Long noise-averaging periods of many hours and even days are usually adopted in order to achieve the necessary accuracy [7]-[10]. Long averaging times help to improve the diffusivity of ambient noise and are expected to enhance the coherent component of the

resulting NCCFs. However, the usefulness of long-term averages is limited when an acoustic environment changes considerably during the noise averaging period. Furthermore, time is of the essence in military operations, let alone in a war. To this end, the goal of this thesis is to accelerate the process of producing high-quality NCCF estimates that can be used to quantitatively characterize the underwater acoustic environment. Achieving ocean characterization using short-term noise averages will greatly enhance the operational relevance of acoustic noise interferometry.

Five chapters are included in the thesis. Chapter II details the methodology used in the research. In Chapter III, we provide the necessary background of the SW06 experiment and present the NCCFs obtained with the data acquired in several observation periods of various duration. Furthermore, in Chapter IV, the promising candidates of NCCFs that are obtained with short noise-averaging times, are employed to retrieve dispersion curves of acoustic normal modes. Chapter V summarizes our conclusions and proposes potential future research.

THIS PAGE INTENTIONALLY LEFT BLANK

II. PASSIVE ACOUSTIC REMOTE SENSING OF THE OCEAN USING NOISE INTERFEROMETRY

A. NOISE INTERFEROMETRY

Noise interferometry (NI) is a technique that allows one to obtain an approximation of Green's functions (GFs) which describes the acoustical properties of an ocean environment. In an active underwater scenario, a Green's function is the acoustic response of a receiver when receiving a signal generated by a compact source. In the noise interferometry context, two hydrophones are employed, one is treated as a virtual source and the other one is a receiver, and vice versa. An approximation to a Green's function retrieved by NI is referred to as an empirical Green's function (EGF). An empirical Green's function is obtained by calculating cross-correlation of time series between two spatially separated hydrophones simultaneously measuring ambient noise. An EGF can be used as a signal to probe an environment and yield characteristic properties of the ocean.

In this work, the calculation of NCCF is done in the frequency domain at first. In frequency f domain, NCCF $\hat{C}(f)$ is calculated by the following Ref. [7], [8], [12]:

$$\hat{C}(f) = \frac{1}{N}\sum_{n=1}^{N}\frac{P_{A,n}(f)P_{B,n}^{*}(f)}{\left|P_{A,n}(f)P_{B,n}^{*}(f)\right|}, \tag{2.1}$$

where $P_{A,n}(f)$ and $P_{B,n}(f)$ are the Fourier transform of acoustic pressure synchronized measured by hydrophones A and B during the n-th non-overlapping time window, N is the number of time windows used in averaging, and an asterisk represents complex conjugation. The pre-whitening process, also known as normalization, is designed to prevent strong, transient non-diffusive noise from contributing disproportionally to NCCFs. In the time-domain, the NCCF $C(\tau)$ is obtained by the inverse Fourier transform of the frequency-domain NCCF $\hat{C}(f)$. An NCCF consists of two copies of EGF; the part of positive time delay corresponds to a sound that propagates from hydrophone A to hydrophone B, and the negative part corresponds in the opposite direction. In this research, we use the software developed by Tan et al. [10] in NCCF calculation.

To achieve sufficient diffusivity of ambient noise, a certain amount of averaging observation period is required. Figure 1 is the NCCFs obtained using different observation periods during the Florida Straits experiment [7]. The peaks of the NCCFs became more evident while a longer observation period was employed. However, the quality of NCCFs degrades when the acoustic properties of the ocean waveguide significantly change during the NCCF averaging observation period. One needs to considerer the trade-off when selecting the averaging observation period in calculating NCCFs.

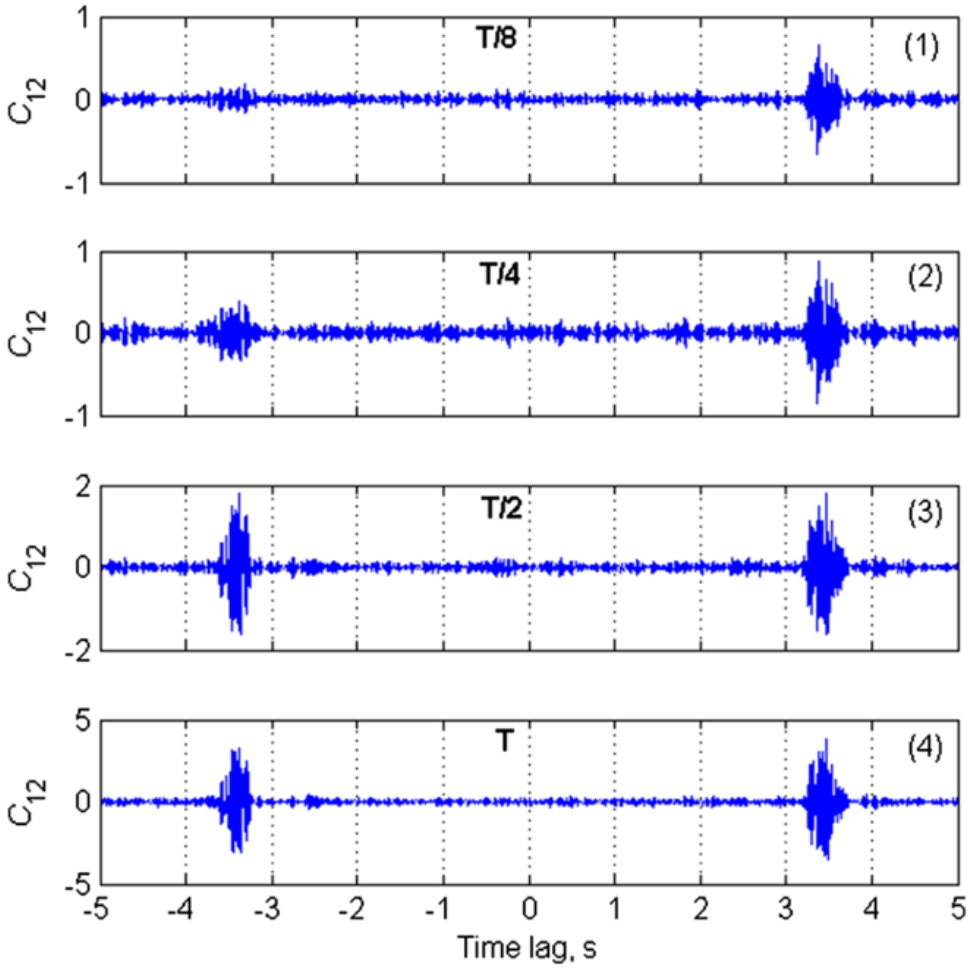

The NCCFs were calculated using various observation periods where the maximum period was about 6 days.

Figure 1. NCCFs averaged over 6 days during the Florida Straits experiment. Source: [7].

B. ACOUSTIC NORMAL MODE DISPERSION CURVES

The usefulness of noise interferometry relies on the accurate retrieval of modal information, i.e., acoustic dispersion curves. Dispersion is the dependence of acoustic wave velocity on frequency. An acoustic dispersion curve of normal modes [13] is a dependence of the group speed on frequency (or travel time if travel distances are known), which implicitly contains environmental information of an ocean waveguide. An ocean waveguide is bound by ocean surface and seafloor and is characterized by the properties of the ocean environment, e.g., water depth, sound speed, and bottom sediment. Theoretically, the modal group speeds converge to the minimum sound speed of an ocean waveguide in the high-frequency region.

There are two advantages of using acoustic dispersion curves to characterize an ocean environment. First, acoustic dispersion curves are sensitive to the subtle variation of the ocean environment. Second, they are independent of the noise spectrum, which means one can exploit acoustic dispersion curves without the precise knowledge of noise properties. Therefore, acoustic dispersion curves are appropriate candidates for acoustically characterizing the acoustic properties of the ocean and its boundaries. The retrieval of dispersion curves from empirical Green's functions is technically challenging due to the intrinsic time-frequency uncertainty and complex modal interference, especially in a shallow water context. To separate the contribution of normal modes from EGFs, we apply the time-warping transform followed the Ref. [14]-[16].

C. TIME-WARPING TRANSFORM

A method called the time-warping transform [17] is a non-linear, invertible signal processing technique. This technique has been widely implemented in a variety of acoustic applications, e.g., geoacoustic inversion [18]. Mathematically, the time-warping transform, i.e., transformation from a time-domain signal $S(t)$ to a warped-time domain signal $\tilde{S}\left(w(t)\right)$, is calculated as [18]:

$$\tilde{S}\left(w(t)\right) = \left|w'(t)\right|^{-1/2} S(t). \tag{2.2}$$

where $w(t)$ is the warping function and t is the acoustic travel time. Time-warping transform has been proven successful in insolating the modal energy from EGFs in shallow-water waveguides [19]. The warping function $w(t)$ is given as [18, 20–22]:

$$w(t) = \sqrt{t^2 - \tau_r^{\,2}}, \tag{2.3}$$

where initial warping time $\tau_r = r/c_w$, r is the distance between two hydrophones, and c_w is the reference group speed of acoustic propagation in free space. Note the reference group speed c_w is the highest observed group speed and subject to change due to acoustic properties of a waveguide. The inversion process of the time warping is to transform each mode signal in the warped-time domain back into a normal time domain. The unwarping function is given by

$$\tilde{w}(t) = \sqrt{t^2 + \tau_r^{\,2}}, \tag{2.4}$$

which is simply obtained by inversing the warping function.

Figure 2 shows the standard time-warping process. Note in Figure 2 (a), the dispersion curves of the received signal (black-line) are drawn only for readers to understand the workflow of modal energy transformation, the normal modes of the received signal are not separated in the original spectrogram. After the successful time-warping transform, modal energy should be separated clearly concerning distinct frequencies in the warped domain (Figure 2 (b)). A proper time-frequency mask, i.e., a modal filter, is applied to isolate the energy of each mode (Figure 2 (c)), preventing spurious non-modal energy in the noise field from falsely contributing to modal dispersion curves. When the separation of modal energy is completed, dispersion curves can be retrieved by inverting the time-warping transform (Figure 2 (d)).

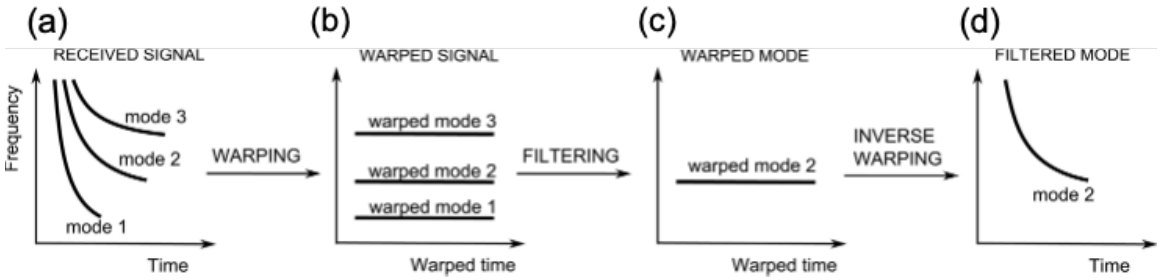

Figure 2. Time-warping transform procedure. Source: [17].

In this research, time-warping is employed to separate normal mode components of measured NCCFs and facilitate the retrieval of dispersion curves of normal modes.

THIS PAGE INTENTIONALLY LEFT BLANK

III. EXPERIMENT DATA PROCESSING AND ANALYSIS

A. SHALLOW WATER 2006 EXPERIMENT (SW06)

The Shallow Water 2006 Experiment, a multi-disciplinary experiment involving several scientific institutions, was conducted on the continental shelf off the coast of New Jersey. The acoustic data recorded by a Single Hydrophone Receiving Unit (SHRU) and SHARK Horizontal Line Array (HLA) are employed in this thesis to perform noise interferometry. The deployed location of the water depth of SHRU and HLA is 75 m and 79 m, respectively. HLA consists of 32 hydrophones and is assigned hydrophone numbers #1 to #32 from north to south, and the horizontal distance between hydrophones is 15 m. The acoustic data measured at SHRU and HLA were collected by Woods Hole Oceanographic Institute (WHOI). The detail of the SW06 experiment was documented by Newhall et al. [23].

A total of 32 paths are formed by SHRU and individual hydrophones of HLA. The NCCFs are calculated based on those 32 paths, which generate 32 NCCFs. The distance between SHRU and HLA is gradually increasing along with the hydrophone number of HLA from approximately 3.4 km for the first path to about 3.8 km for the last path (Figure 3). For brevity, i-th NCCF represents the NCCF is calculated between SHRU and i-th hydrophone of HLA.

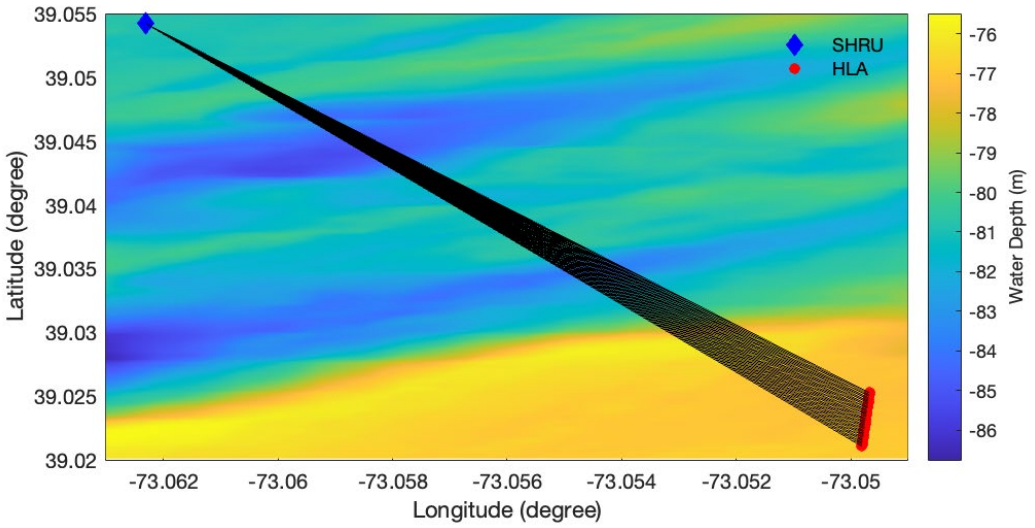

The horizontal projection of acoustic travel path between SHRU and each hydrophone of HLA. Bathymetry at the SW06 site is shown by color.

Figure 3. SW06 Experiment site with the location of SHRU and HLA used in this study

The acoustic data used in this thesis contain 15-day-long shipping and ambient noise starting from 18 August to 1 September. Note that the time used in this thesis is referred to as GMT time. During this period, strong temporal variability of sound speed was observed (Figure 4 (b)). These rapid changes in the acoustic environment were caused by strong nonlinear internal activity including nonlinear internal gravity waves generated at shelf break. The sound speed shown in Figure 4 was measured at a location near the first hydrophone of HLA and only down to 77 m water depth. Linear extrapolation is applied to estimate the sound speed close to the seafloor.

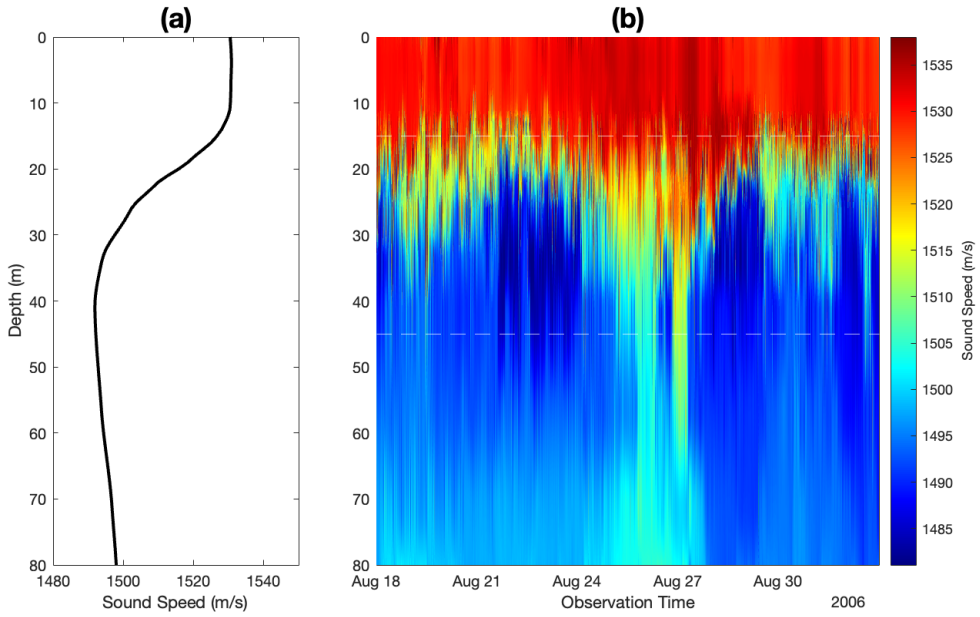

(a) The average sound speed profile over the 15-day observation period. (b) The time series of sound speed (shown by color) at different water depths exhibits the high variation of sound speed especially within the thermocline located from 15 m to 45 m (white dashed line).

Figure 4. Sound speed variation and averaged sound speed profile during the SW06 experiment

Despite the sound speed time dependence shown in Figure 4, a particularly strong internal wave event was observed at the SW06 site on 19 Aug. 2006 (Figure 5). This issue becomes problematic when it happens during NCCF averaging period.

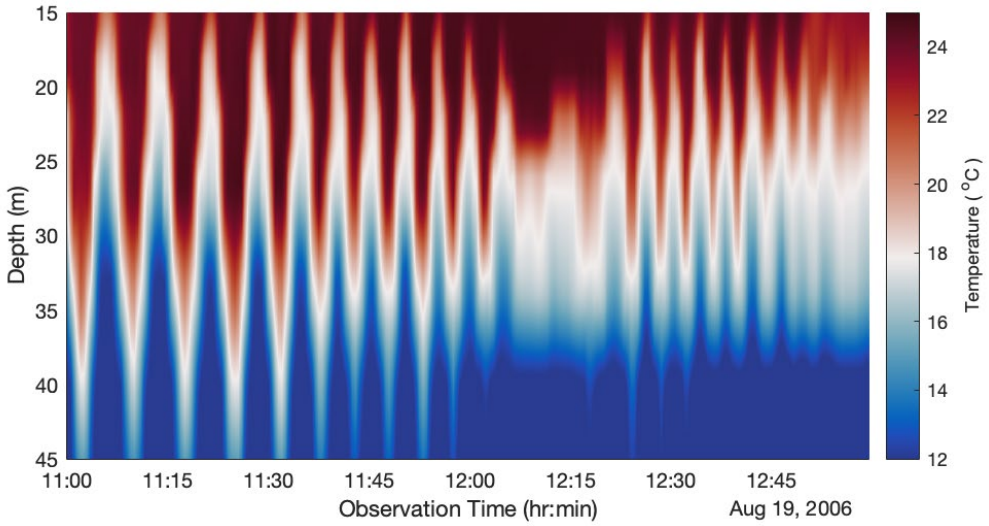

Figure 5. Temperature variation due to the manifest of strong nonlinear internal gravity waves on 19 Aug. 2006

B. NOISE CROSS-CORRELATION FUNCTION

Noise cross-correlation functions (NCCFs) retrieve the coherent components of noise propagating through two receivers. A single NCCF consists of two parts, positive and negative time delay τ. For brevity, the terms of positive and negative parts of an NCCF are abbreviated as P-NCCF and N-NCCF, respectively. In an NI scenario, one can imagine that ambient noise is passing one of the hydrophones at the origin of time delay and travels to the other hydrophone. In this study, the travel direction of P-NCCFs is from SHRU to one of the hydrophones of HLA and the opposite direction goes for N-NCCFs. The NCCFs are derived from the noise propagating between SHRU and 32 hydrophones of HLA, thus 32 NCCFs were generated in this experiment.

With sufficiently diffusive noise, clear and symmetric peaks are formed at both P-NCCFs and N-NCCFs. Those peaks occurred at the time delay approximating the travel time of different frequency components of acoustic normal modes between the two receivers. In NCCF calculation, we follow [10] to apply the 10–110 Hz bandpass filter. The 21st NCCF averaged over the 15-day observation period starting from 18 Aug. is shown in Figure 6 as an example. The abbreviation 15-day NCCF is intensively used for brevity, and the same format of abbreviation is also used for other observation periods.

With the 15-day averaging, the proper diffusivity of the ambient noise and clear NCCF peaks were achieved. The positions of main peaks and troughs in P-NCCF and N-NCCF are expected to coincide due to acoustic reciprocity. However, the details of P-NCCF and N-NCCF are not expected to coincide due to the difference in frequency and modal spectra of noise propagating to and from shore on the continental shelf.

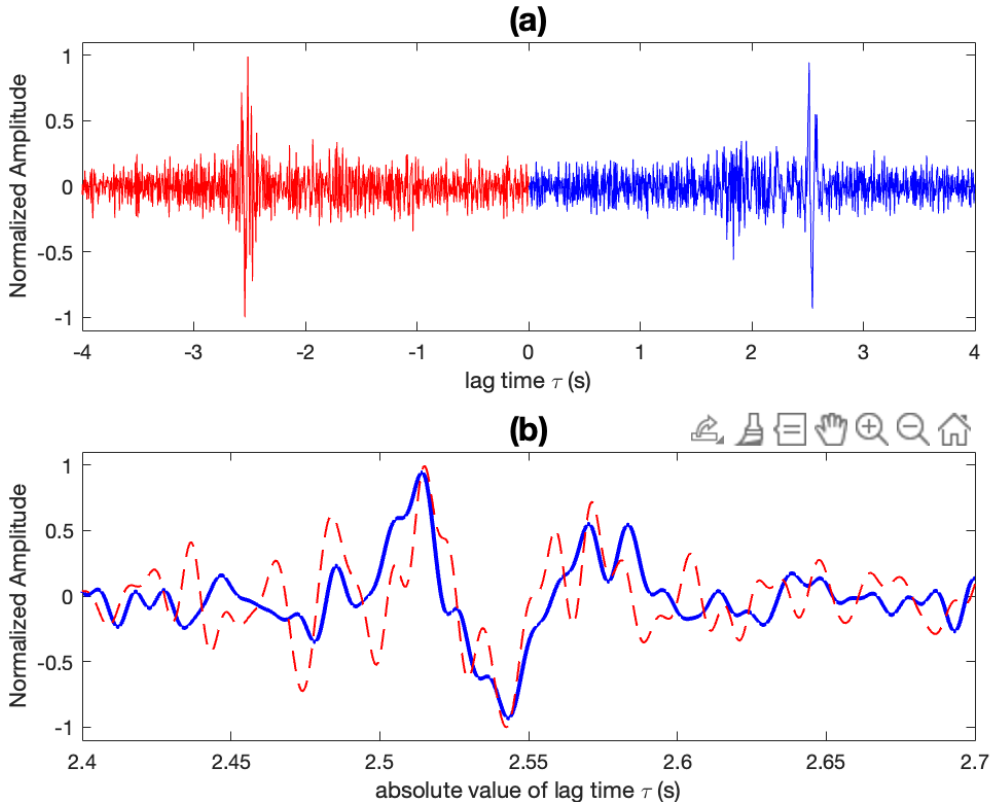

(a) The positive part (blue) and negative part (red) of the 21st NCCF have strong peaks at $\tau \approx \pm 2.5$, corresponding to the acoustic travel time between two hydrophones. (b) Both positive (blue) and negative (red) parts are plotted as a function of the absolute value of lag time τ, showing a similar propagation pattern.

Figure 6. Two-point 15-day noise cross-correlation function between SHRU and HLA hydrophone #21

Figure 8 shows the NCCFs are plotted as a function of time delay and hydrophone number. Mathematically, time delay τ is the time shift between two received signals; the hydrophone number indicates which hydrophone is used in NCCF calculation. Physically, time delay τ represents the travel distance and direction of acoustic propagations;

hydrophone number describes the distance between hydrophones because they were deployed along a straight line at a fixed inter-hydrophone distance of 15 m. Note that the systematical shift of the main peaks toward large $|\tau|$ with the increasing range in Figure 7.

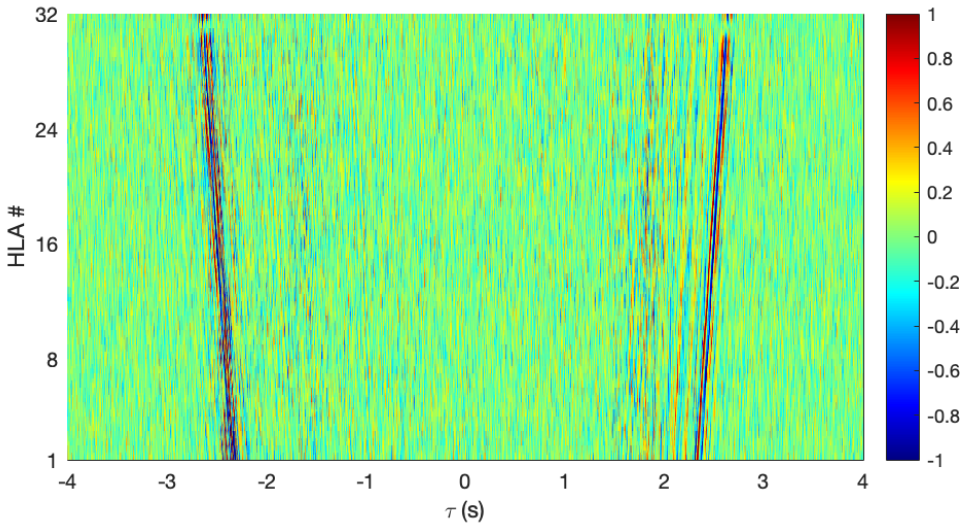

The 15-day NCCFs between SHRU and 32 hydrophones of HLA are plotted as functions of time delay τ and hydrophone number. The normalized magnitude is shown in color bar.

Figure 7. 15-day NCCFs between SHRU and individual 32 hydrophones of HLA

The 31st hydrophone of HLA was determined to be defective throughout the SW06 experiment [23] and thus only the other 31 NCCFs are considered in the subsequent NI process. Furthermore, P-NCCFs exhibit additional peaks that precede the matin peaks (Figure 8). Those unwelcome peaks are believed to be non-diffusive noise from a certain shipping lane of the New York Harbor [10], [24] and led to a partial overlap on the main peaks. The overlap cannot be separated and thus complicates the subsequent NI analysis. N-NCCFs are more suitable than the P-NCCFs for retrieving empirical Green's functions. Therefore, this study focuses on N-NCCFs.

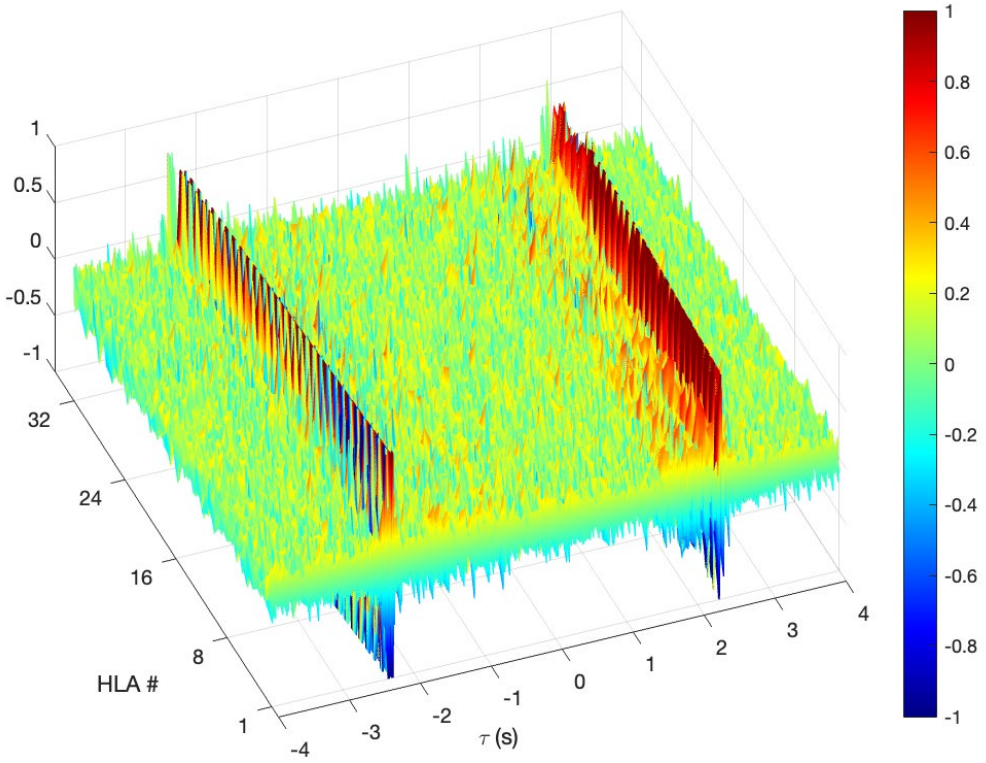

Same as Figure 7 but in 3-D presentation. The strong spurious arrivals roughly manifest at $\tau \approx 1.8$ and partially distort the main peaks of P-NCCFs.

Figure 8. Additional peaks in 15-day P-NCCFs

The advantage of increasing noise diffusivity by extending the NCCF averaging observation period is limited by a difficult acoustic environment, e.g., rapidly changing sound speed. In Section III.C., we search for NCCFs of short observation periods emerging in this challenging experimental site in order to assess the feasibility of using short-time NCCFs to characterize the littoral ocean.

C. SELECTING SHORT-TIME NCCF

In this section, NCCFs are averaged over three different temporal durations using the same experimental geometry for 15-day NCCFs. The three durations include (1) one day, (2) one hour, and (3) 10 minutes. These three durations of time are meant to be diverse to discuss the influence of different time scales. Nevertheless, it is nearly impossible to do an exhaustive search and perform NI over thousands of N-NCCFs. Thus, a selection process is needed to find the most representative ones. The selection process is designed to

find NCCFs of which period can properly estimate GFs. Tan et al. [10] have demonstrated the capability of performing NI using N-NCCFs averaged over 15 days starting from 18. Aug. 2006. As a result, the same 15-day N-NCCFs are used to assess the quality of short-time NCCFs for the selection process. Additionally, a nested process is used to reduce the complexity of selection, e.g., a selected 10-min observation period is inside a selected one-hour period, etc.

The Pearson coefficient [25] is the most common indicator used in determining the correlation between two signals. In the selection process, the Pearson coefficient is introduced to statistically quantify a correlation between N-NCCFs averaged over selected temporal durations and the 15-day N-NCCFs. For each temporal duration, the Pearson coefficient averaged from 31 NCCFs, is an important factor to finalize the period of selection. Besides, a statistical tool called box plot [26] is adopted in Figure 9-Figure 11. The box plot details the coefficient distribution of 31 NCCFs, i.e., the edges of boxes are the 25^{th} to 75^{th} percentile of input data, the whiskers extend to the most extreme data points the algorithm considers to be not outliers, and the outliers which are shown by red dots.

In short, the averaging observation periods with high and consistent Pearson coefficients are promising candidates. For example, the one-day N-NCCFs starting from 23 Aug. show (Figure 9) the highest averaged Pearson coefficient of 0.79, the narrowest box, and no outliers and thus is selected as the one-day representative. On the other hand, the N-NCCFs of 29 Aug. show a comparable averaged Pearson coefficient of 0.71 with a narrow box but is deemed to be less promising due to the several outliers, which means the N-NCCFs are inconsistent among 31 NCCFs.

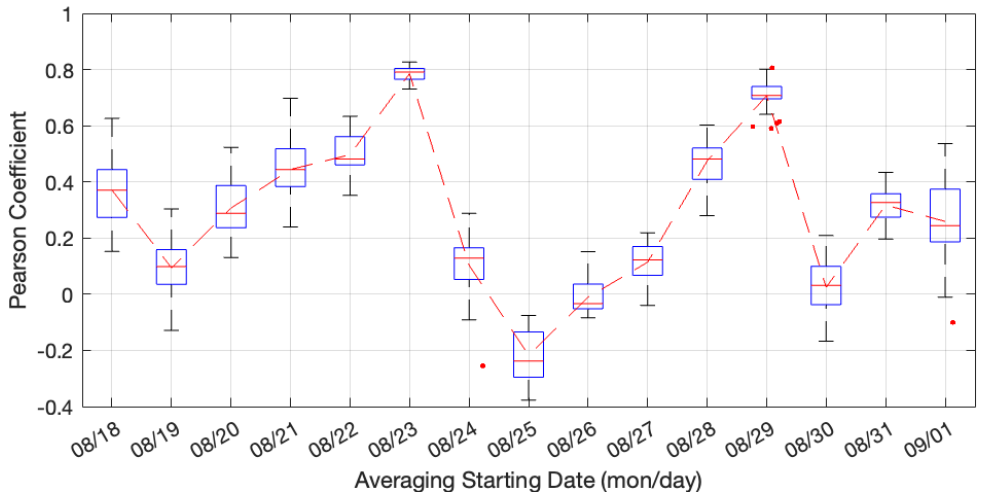

The average Pearson coefficients (red dashed line) and the statistical characteristic of the Pearson coefficients distribution were plotted as a function of date.

Figure 9. Correlation coefficient between one-day N-NCCFs and the 15-day N-NCCFs

In the same manner of selection, the one-hour N-NCCFs starting from 23 Aug. 00:00:00 (Figure 10) and the 10-min N-NCCFs starting from 23 Aug. 00:36:00 (Figure 11) stand out above the rest. Note that the selected one-hour period is starting from 00:26:00 to 01:26:00, the acoustic data of the first 26 minutes were not recorded on 23 Aug. The three selected observation periods of 10-min, one-hour, and one-day are studied in more detail later.

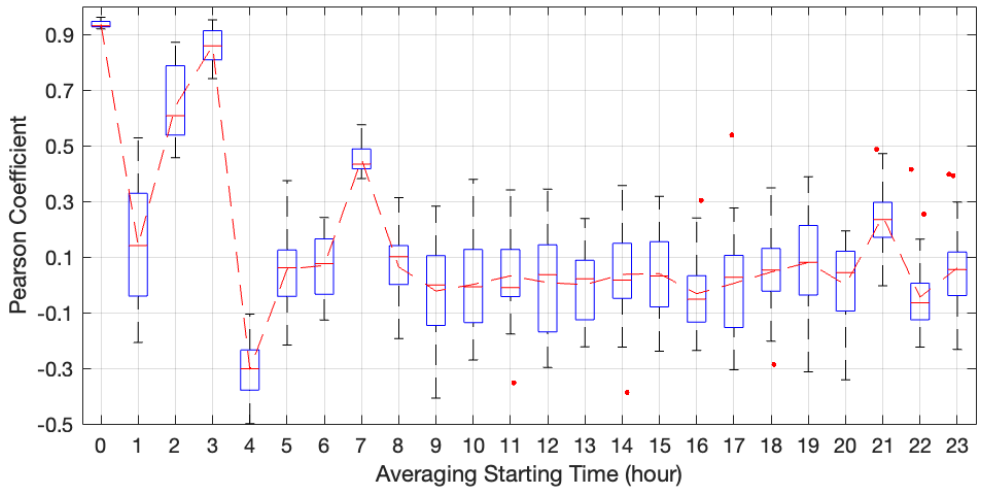

Same as Figure 9.

Figure 10. Correlation coefficient between one-hour N-NCCFs and the selected one-day N-NCCFs

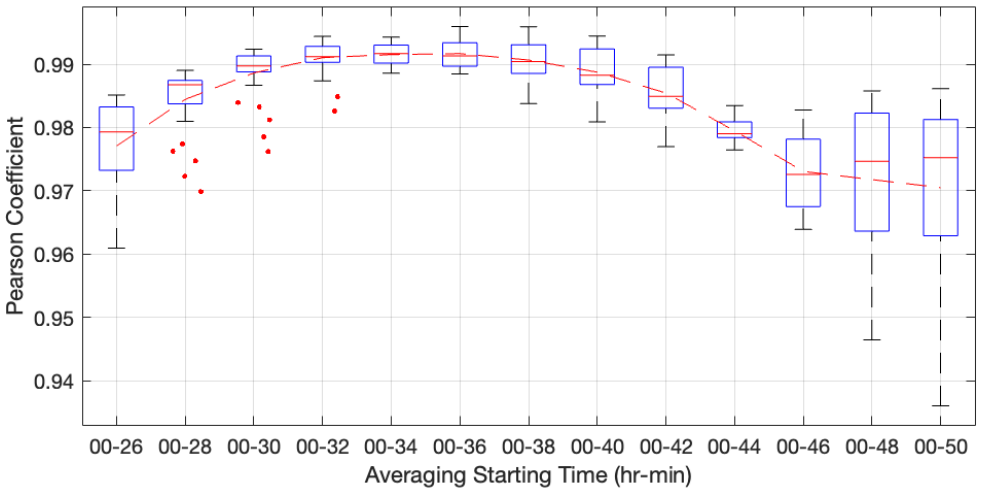

Same as Figure 9.

Figure 11. Correlation coefficient between 10-min N-NCCFs and the selected one-hour N-NCCFs

D. DISCUSSION OF NCCFS OBTAINED WITH SHORT AVERAGING PERIOD

The NCCFs of the four selected observation periods are demonstrated in Figure 12 and Figure 13. Figure 12 exhibits the NCCFs averaged over 15 days and one day, showing clear peaks at both the positive and negative time delay as expected, which is corresponding to a representative acoustical travel time between hydrophones of HLA and SHRU.

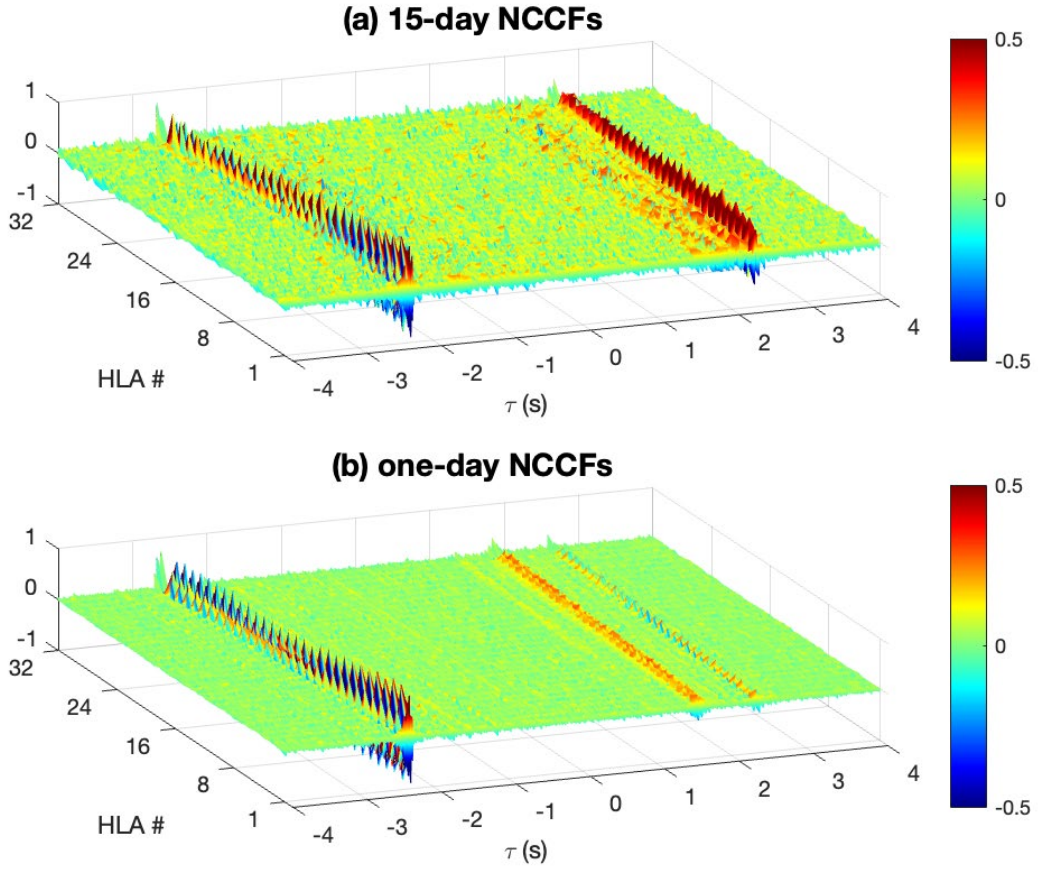

Same as Figure 8.

Figure 12. NCCFs of 15-day and one-day observation period

However, the absence of positive peaks for two short-time NCCFs (Figure 13) raises a hypothesis that a strong non-diffusive source was present closed to the site of interest and contributed to the cross-correlation functions. Thus, further investigation is required to validate the NCCFs obtained in the 10-min and one-hour observation period.

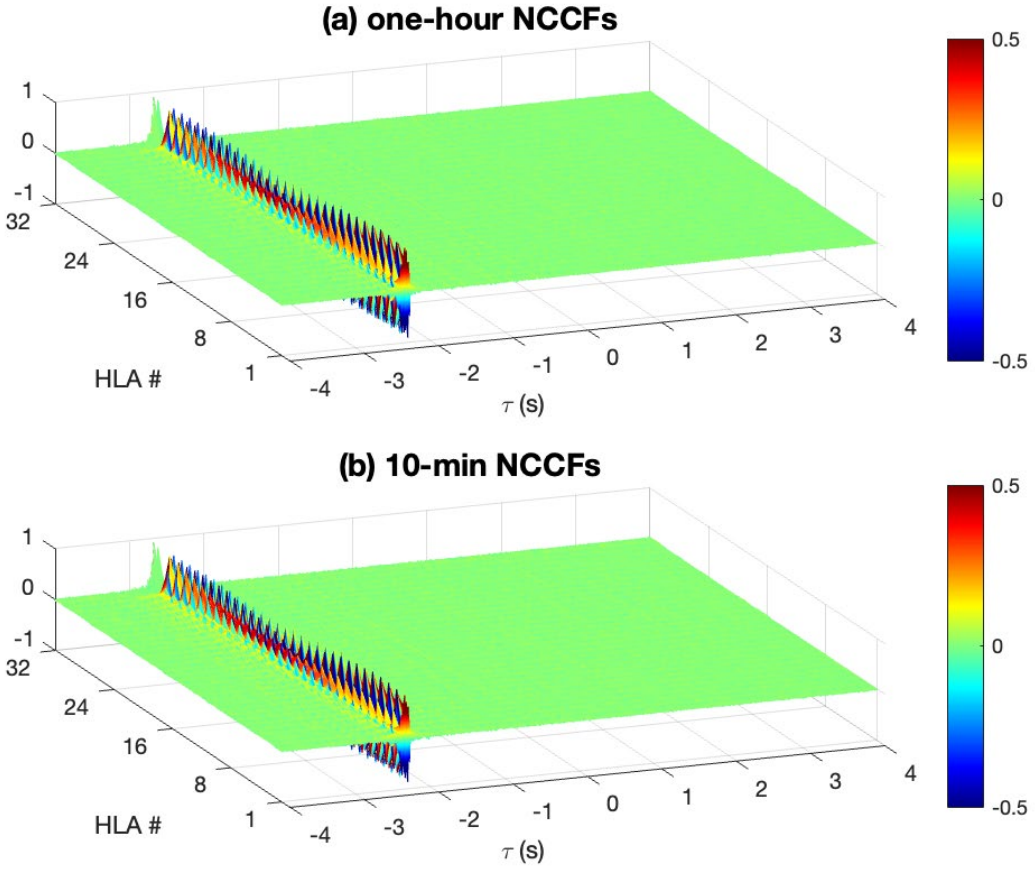

Same as Figure 8.

Figure 13. NCCFs of one-hour and 10-min observation period

The spectrogram of the selected one-hour observation period (Figure 14) is used to check if any non-diffusive source manifested during this observation period. Figure 14 displays the strong broadband signals are at 224 ± 8 Hz, 300 ± 30 Hz, and 400 ± 50 Hz. Those signals are identified to be the sources deployed by Woods Hole Oceanographic Institution (WHOI) and Navy Research Lab (NRL) during the SW06. Both sources were transmitting for 7.5 minutes every 30 minutes [23]. As mentioned, the 10 Hz - 110 Hz bandpass filter is applied in NCCF calculation, so none of those sources are contributing to the NCCFs.

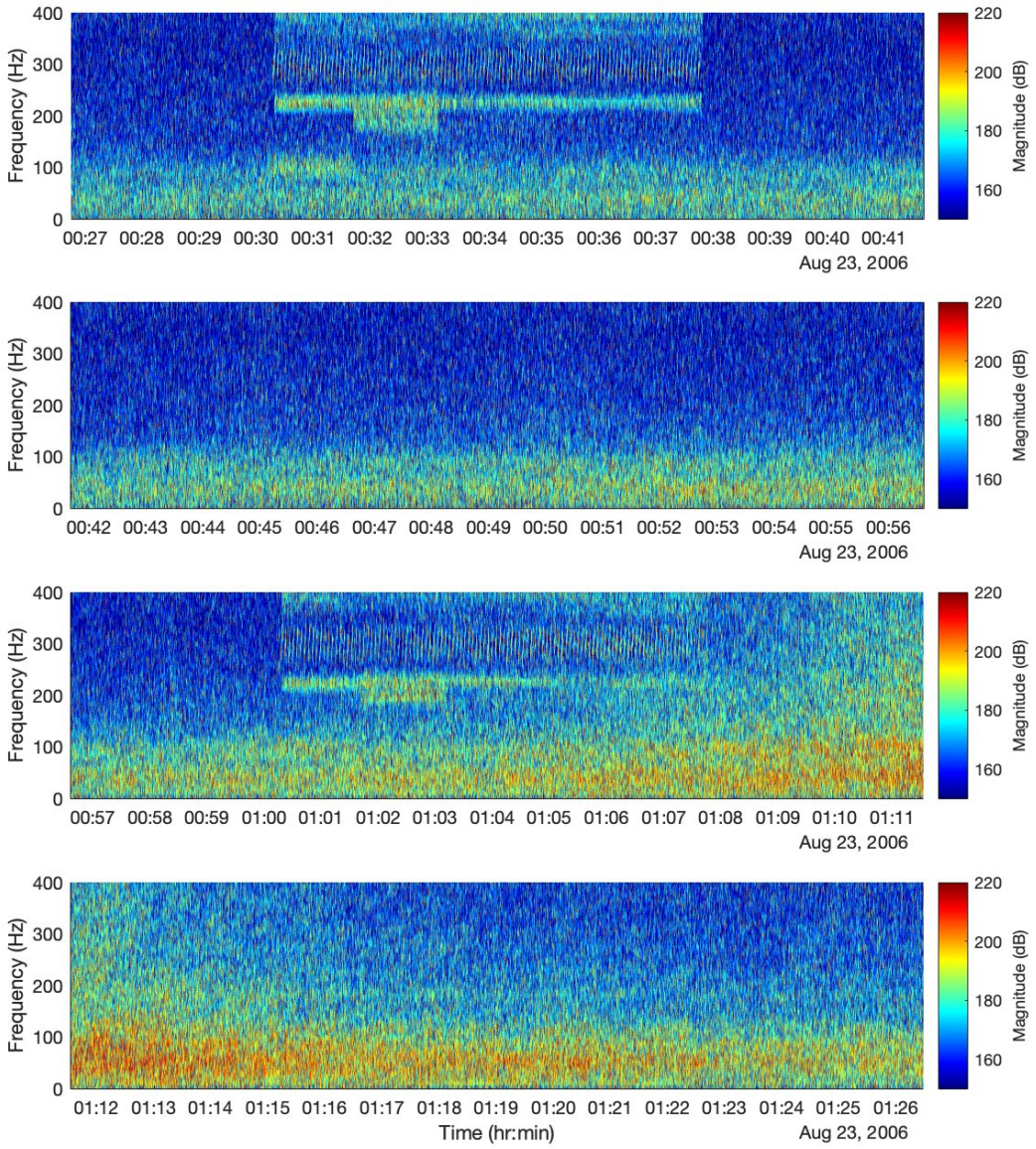

The spectrogram of one-hour acoustic data recorded at SHRU from 00:26:00 to 01:26:00 23 Aug. Each panel contains 15-min spectrogram.

Figure 14. Spectrogram of the acoustic data recorded at SHRU during the selected one-hour observation period

Also, the spectra (Figure 15) show no indications of any strong controlled sources below 110 Hz. The energy below 110 Hz is mostly from ambient and distant shipping noise, which is desired for performing passive noise interferometry.

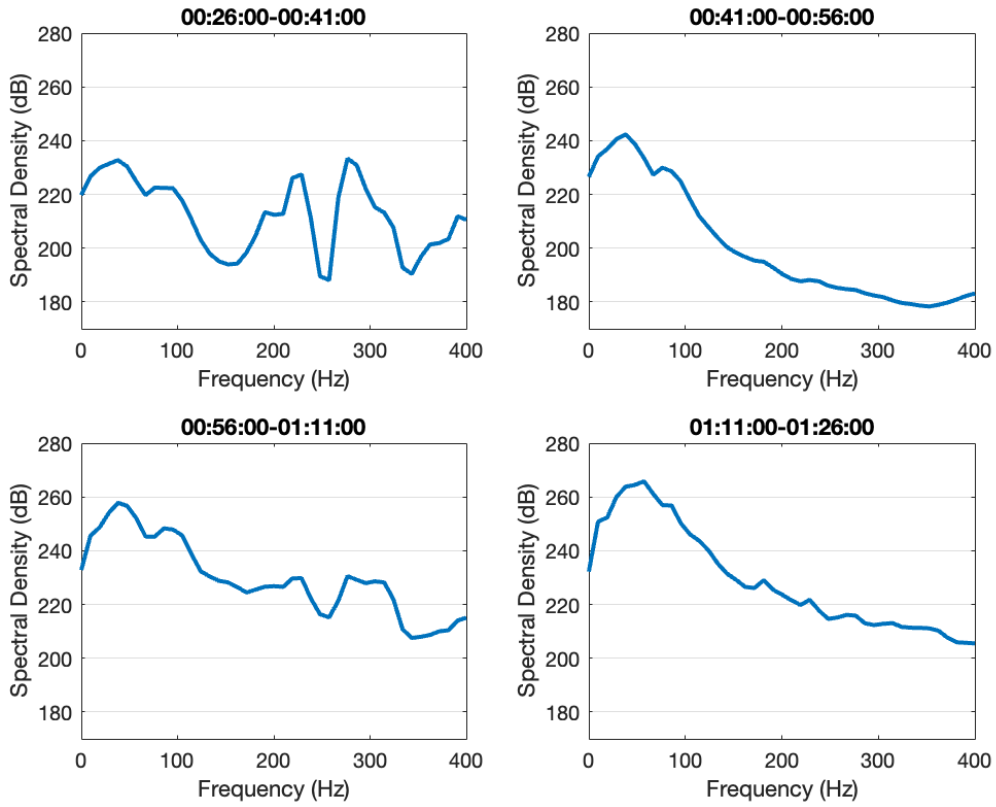

The corresponding spectral density to each 15-min spectrogram in Figure 14.

Figure 15. Energy density of acoustic data recorded at SHRU during the selected one-hour observation period

However, the top and bottom panels in Figure 14 show two broadband signals at 101.7 ± 12.5 Hz and 203.5 ± 25 Hz. These two signals are from an active source used in SW06, the Miami Sound Machine (MSM), transmitting for 90 seconds every 30 minutes [23]. The signal at 101.7 ± 12.5 Hz is under our concern. Assumed a signal propagates at a group speed of 1490 m/s, the distance between MSM and SHRU, MSM and the first hydrophone of HLA, MSM and the last hydrophone of HLA is 17.1 km, 19.3 km, and 19.7 km, respectively (Figure 16). By simple calculation, the estimated peaks of NCCFs, if any, are likely at the positive time delay $\tau \approx 1.5 - 1.8$ s, which explains the earlier peaks of the selected one-day P-NCCF in Figure 12 (b). Thus, the source from Miami Sound Machine is not contributing to N-NCCFs.

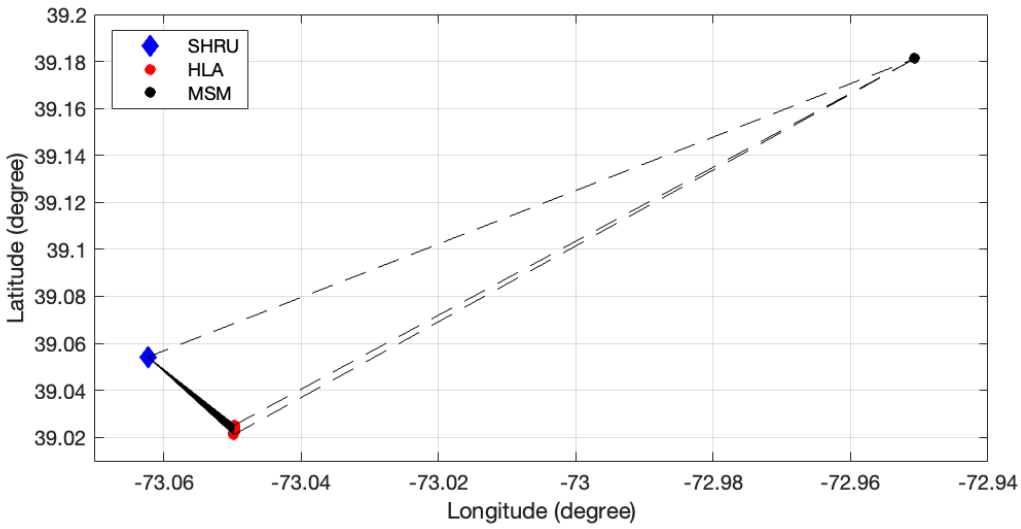

Figure 16. Locations of Miami Sound Machine, SHRU, and hydrophones of SHARK HLA

THIS PAGE INTENTIONALLY LEFT BLANK

IV. APPLICATION OF TIME WARPING TRANSFORM TO SHORT-TIME NCCFS

A. TIME-WARPING TRANSFORM

In this section, we apply the time-warping transform to 15-day NCCFs and selected short-time NCCFs to facilitate the retrieval of corresponding acoustic dispersion curves. Obtaining acoustic dispersion curves is technically challenging because the ocean is complicated and variable. In short-range propagation context, without time-warping transform, the complex modal interference hinders the extraction of acoustic dispersion curves (Figure 17).

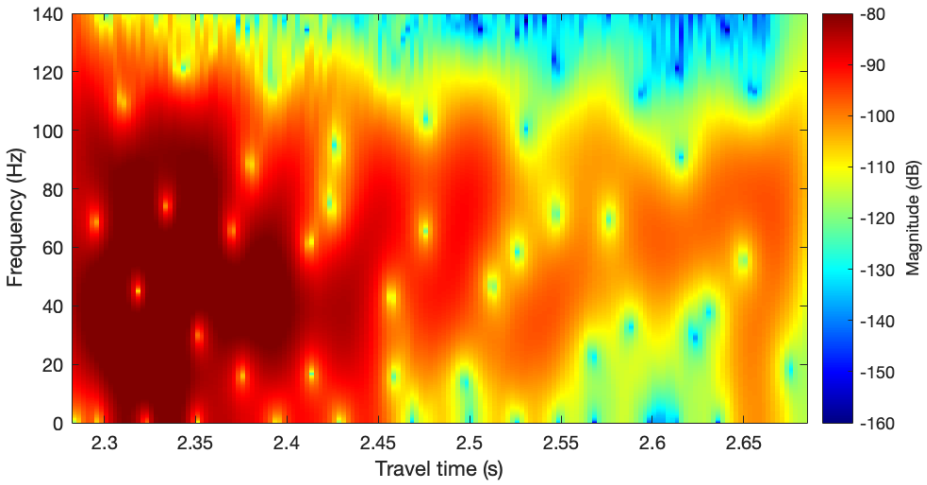

The spectrogram of one-day N-NCCF reveals the complexity of the ocean and acoustic interference by individual modes. The modal information is not clear in the original spectrogram and cannot be obtained directly.

Figure 17. Original spectrogram of one-day N-NCCF

With an appropriate time-warping transform, modal energy, theoretically, is horizontally separated in warped-frequency domain and easily identified. However, it is not the case when the acoustic data of the real ocean come into play. First, time-frequency masks for isolating individual modes change subtly but significantly in different scenarios. Second, determining the earliest time of signal arrivals is critical to precisely retrieved modes and dispersion curves. An early or late arrival time for time-warping transform leads

to an inaccurate spectrogram in the warped domain and increases the ambiguity of energy distribution between modes. These two issues are studied and discussed in this section.

1. Time-Frequency Mask Design

Traditionally, the design of time-frequency masks is done manually and visually, which is highly subjective. To compare the performance between NCCFs averaged over the selected observation periods, objective masks are required to exclude any personal preference. To begin with, the energy between modes, which is possibly caused by spurious non-diffusive signals, can be comparatively strong and thus deceptive (Figure 18 (a)). By averaging the spectrograms of the 31 NCCFs, the deceptive energy is significantly decreased (Figure 18 (b)). This averaging method successfully suppresses the possible contribution of non-diffusive signals and enhances modal energy, i.e., the edge sharpness considerably increases, which facilitated the identification of modes.

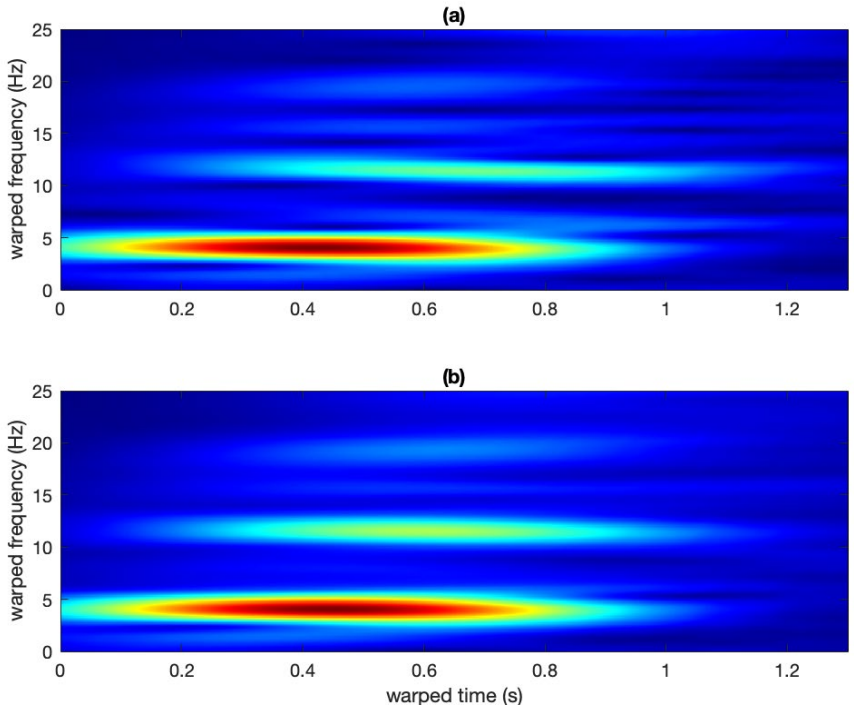

(a) The warped-domain spectrogram of only one N-NCCF exhibits the confusing energy between mode#2-3. (b) The warped-domain spectrogram averaged from 31 NCCFs shows more energetic modes and clear modal boundaries.

Figure 18. Spectrogram of only one NCCF and averaged NCCF in warped domain

The averaging method is also conducted in the spectral domain. Figure 19 shows the averaged spectra of 31 NCCFs in warped domain provide the most energetic frequencies with respect to each mode. Those frequencies are referred as center frequencies for our mask designing. The results of the center frequency for different observation periods are shown in Table 1.

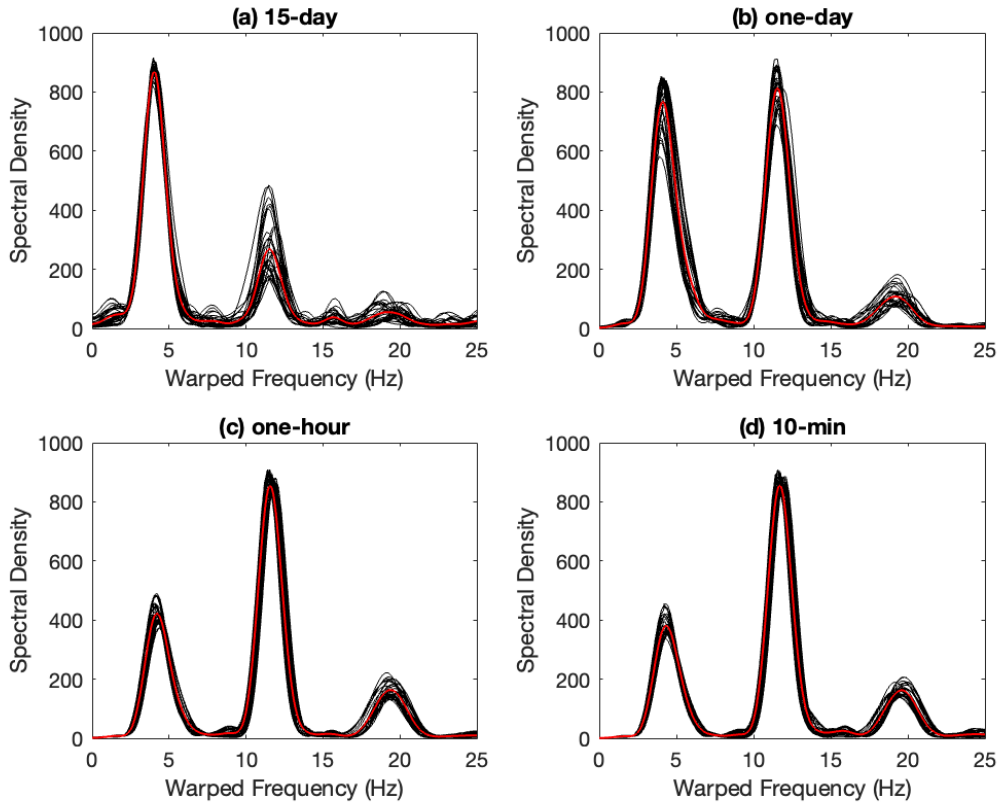

The spectra of 31 NCCFs in the warped domain are shown by black line and the averaged spectra of 31 measurements are shown by red line. Each panel represents different observation periods which are specified by corresponding titles.

Figure 19. The spectral density of N-NCCFs in warped domain

Table 1. Center frequencies of normal mode frequency bands for different observation periods

Mode #	15-day NCCF	One-day NCCF	One-hour NCCF	10-min NCCF
1	4.05 Hz	4.18 Hz	4.25 Hz	4.38 Hz
2	11.56 Hz	11.56 Hz	11.58 Hz	11.71 Hz
3	19.31 Hz	19.18 Hz	19.38 Hz	19.58 Hz

After determining the center frequencies, a reasonable bandwidth is required to include most of the modal energy. The principal rule is to capture most of the modal energy and least of the noise energy. With the averaging spectrograms which enhanced the contrast visually, 3.5 Hz (±1.75 Hz from the center frequencies) in the warped domain is a reasonable bandwidth. Thus, the ultimate time-frequency masks are finalized for each observation period (Figure 20) and used for the subsequent isolation process of modes.

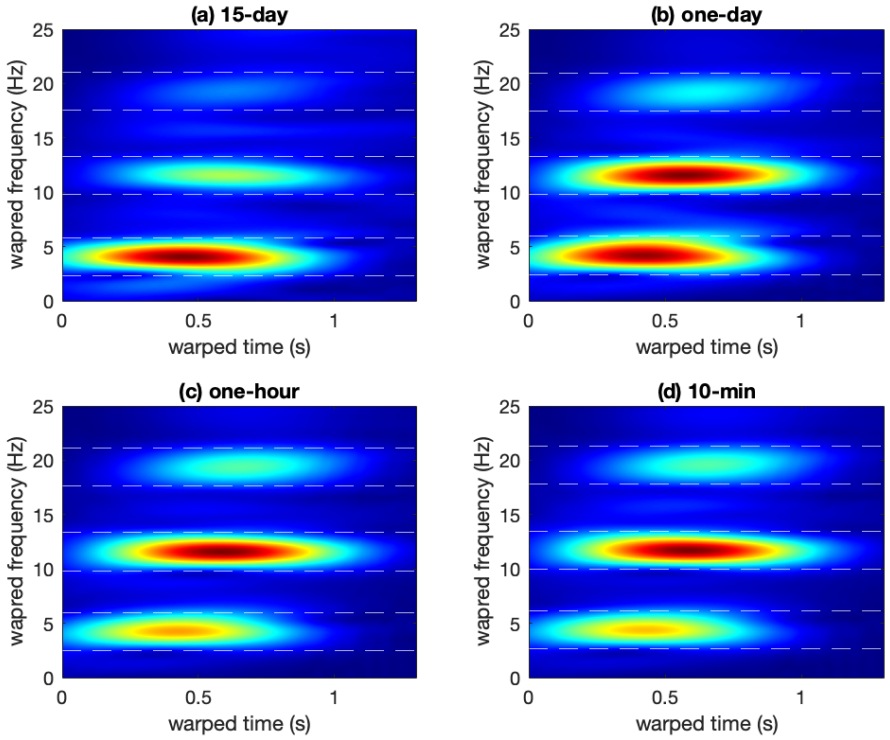

The finalized masks (white-dashed line) based on center frequencies and 3.5 Hz bandwidth. Each panel represents different observation periods that are specified by corresponding titles.

Figure 20. The time-frequency masks for NCCFs.

2. Determination of the Earliest Signal Arrival Time

The parameter τ_r in the warping function has the meaning of the first arrival time of a signal, which is given by $\tau_r = r/c_w$ where r is the distance between SHRU and individual hydrophone of HLA and c_w is the reference group speed of acoustic propagation. Thus, the reference group speed c_w is the highest observed group speed and depends on the acoustic properties of the ocean. An accurate estimation of arrival time is important to a successful time-warping process (Figure 21 (a)(b)), while poor estimation of arrival time leads to unsatisfactory separation of modes (Figure 21 (c)(d)) or losing the energy of the first mode (Figure 21 (e)(f)).

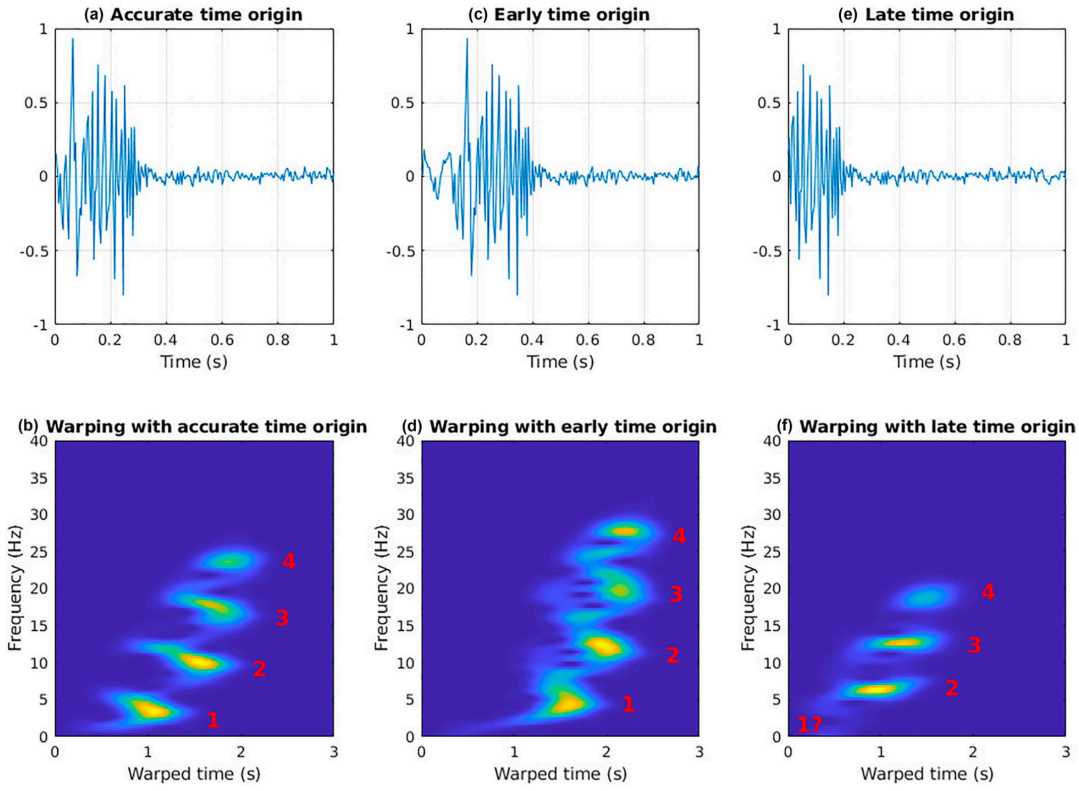

The comparison of time-warping results with different sound speeds c_w in the warping function (Equation (2.2)). (a) accurate estimation of c_w and (b) spectrogram showing a proper mode separation. (c) overestimated c_w and (d) spectrogram showing an unclear mode separation. (e) underestimated c_w and (f) spectrogram showing the absence of the first mode.

Figure 21. Effects of selecting an inaccurate sound speed c_w. Source: [17]

In this research, the distance r is approximately from 3.4 km to 3.8 km. Also, the locations between SHRU and hydrophones of HLA are assumed to remain unchanged throughout the selected observation period. The reference group speed c_w is the key to determining the signal arrival time τ_r. To find accurate reference group speed c_w, time-warping is implemented in NCCFs using different c_w. The span of c_w range from 1480 m/s to 1500 m/s, which is a relatively wide estimation. With proper masks discussed in Subsection IV.A.2, we determine which reference group speed c_w can bring the most energy falling into modal masks.

The results shown in Figure 22 are based on the ratio calculated between the mode energy and the total energy below 25 Hz in the warped-frequency domain. The term mode energy refers to the energy of the first three modes because the energy of mode order > 3 is relatively weak and thus negligible. Figure 22 shows the best performance of the time-warping happens at $c_w = 1487$ m/s for the 15-day NCCFs, $c_w = 1488$ m/s for the one-day NCCFs, $c_w = 1489$ m/s for the one-hour NCCFs and $c_w = 1490$ m/s for the 10-min NCCFs. These c_w values are used in the time-warping transform.

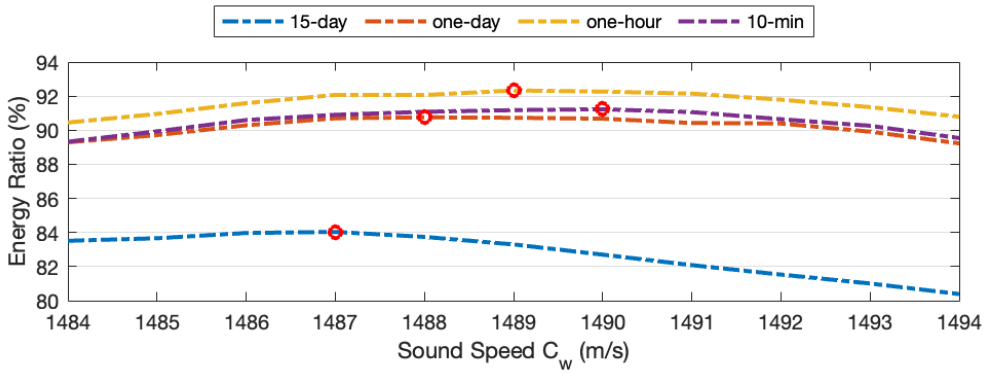

The percentage of captured energy that is represented by the low-order modes #1-3 is shown as a function of reference group speed c_w (colored dashed-line). The optimum c_w values correspond to maximum captured modal energy and are highlighted by red circles.

Figure 22. Selection of the reference group speed c_w in the time-warping transform

3. Modal Energy Distribution and Signal Restoration

Figure 22 shows not only optimum c_w values but also the corresponding ratios of extracted energy. The corresponding ratios reveal the NCCFs averaged over the longest observation period have more energy leakage than the NCCFs with short-time noise averaging. This result makes long averaging time less appealing because the unwarping process is applied to the time-frequency domain specified by the modal masks, i.e., the energy outside masks in the warped domain is not contributing to the unwarping results. Concisely, the more energy is captured by modal masks while time-warping, the more representative of oceanic characteristics the unwarping results can be.

In Table 2, the energy ratio of the 15-day NCCFs is only 84.1%. On the other hand, the ratio is up to 92.2% in the one-hour NCCFs. The acoustic properties of an ocean waveguide change as well as modal parameters. Thus, employing a long averaging observation period results in higher energy loss. Moreover, the information of high-order modes is relatively valuable and usually hard to acquire due to significant transmission loss. The energy ratio of mode #3 increases from 5.1% of the 15-day NCCFs to 13% of the one-hour NCCFs. As a result, one can expect that a short averaging period used in NCCF calculation improves the overall extraction of modal energy, especially for high-order modes.

Table 2. Ratio of modal energy captured in selected NCCFs

Mode #	15-day NCCF	One-day NCCF	One-hour NCCF	10-min NCCF
1	60.1%	41.3%	27.5%	25.5%
2	18.9%	42.4%	52.1%	53.0%
3	5.1%	7.1%	12.6%	12.9%
Total	84.1%	90.8%	92.2%	91.4%

Once the energy of each mode is isolated in the warped domain, it can be inverted to the physical time domain by the unwarping transform (Equation (2.4)). The unwarping result of one-hour NCCF is shown in Figure 23 as an example. The waveforms of the first three modes are successfully extracted from the one-hour N-NCCF. The restored signal,

i.e., the combination of the first three modes, exhibits only a small difference compared to the original one-hour N-NCCF (Figure 23).

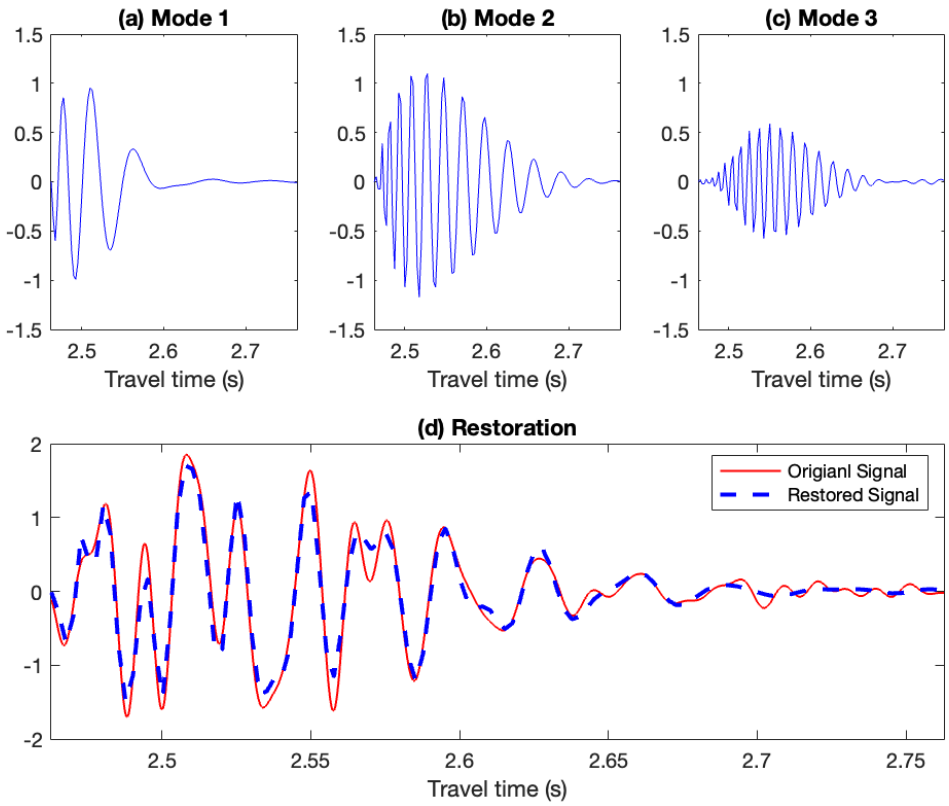

Normal mode components of the 20th one-hour NCCF are shown in the time domain in panel (a)-(c). In panel (d), the sum of the first three modes superimposed (blue-dashed line) closely reproduces the measured NCCF (red line).

Figure 23. NCCF restoration from the first three unwarped modes

B. NORMAL MODE DISPERSION CURVES

1. Retrieval of the Dispersion Curves

With proper modal masks and accurate reference group speed, the time-warping and unwarping processes are demonstrated in Figure 24 (a)-(c) as an example. Then we apply short-time Fourier transform to unwarped modes and retrieve corresponding normal mode dispersion curves by finding the travel time that provides the greatest magnitude of the spectral density in each frequency bin (Figure 24 (d)).

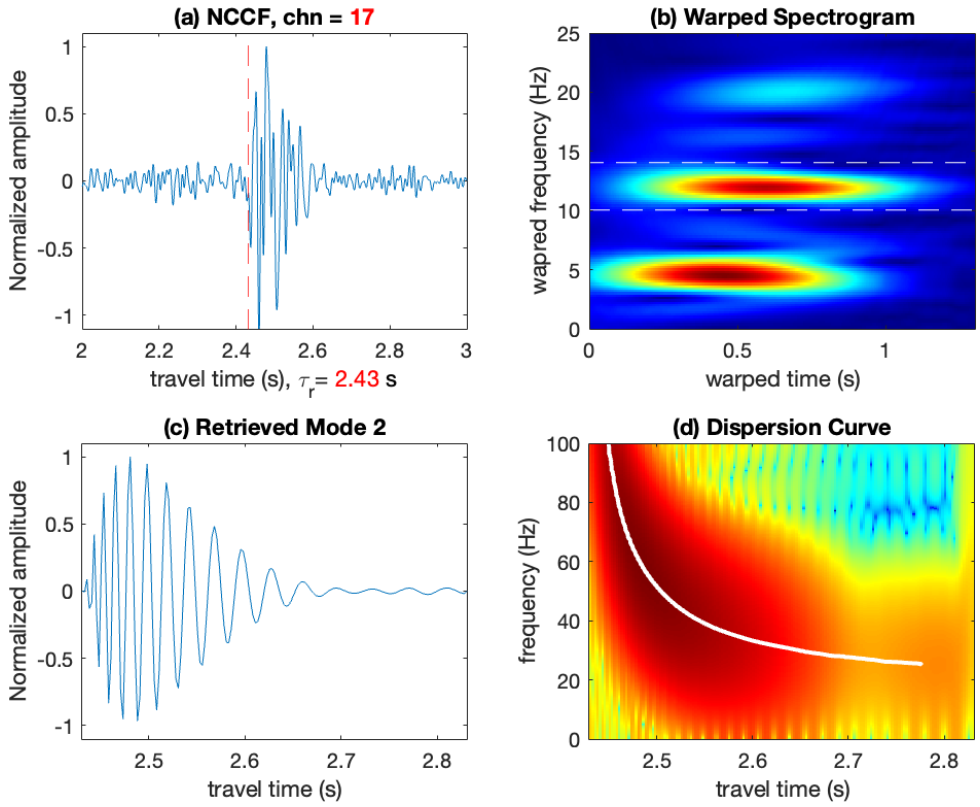

The application of the time-warping and unwarping process in one-day N-NCCF: (a) N-NCCF (blue line), the warping starts at $\tau_r = 2.43$ s (red-dashed line) (b) Spectrogram in warped domain with the mask isolating mode #2 (white-dashed line) (c) Retrieved mode #2 in the time domain (d) Spectrogram of mode #2 in time-frequency domain with the retrieved dispersion curve of mode #2 (white line).

Figure 24. Application of the time-warping and unwarping transform to the one-day N-NCCF

Normal mode dispersion curves can be presented as a dependence of frequency on travel time t_m or group speed g_m. The group speed is given by $g_m = r/t_m$, where r is the distances between SHRU and hydrophones of HLA. The dispersion curves of the first three modes as a function of group speed are shown in Figure 25-Figure 27, respectively.

2. Dispersion Curves Analysis

In Figure 25-Figure 27, we define three regions: low-frequency, mid-frequency, and high-frequency, and discuss them separately. In the low-frequency region, the dispersion curves tend to bounce back where the corresponding group speeds are close to

the minimum [27], which is unphysical. This is attributed to the intrinsic limitation of the time-warping transform and not discussed in this thesis.

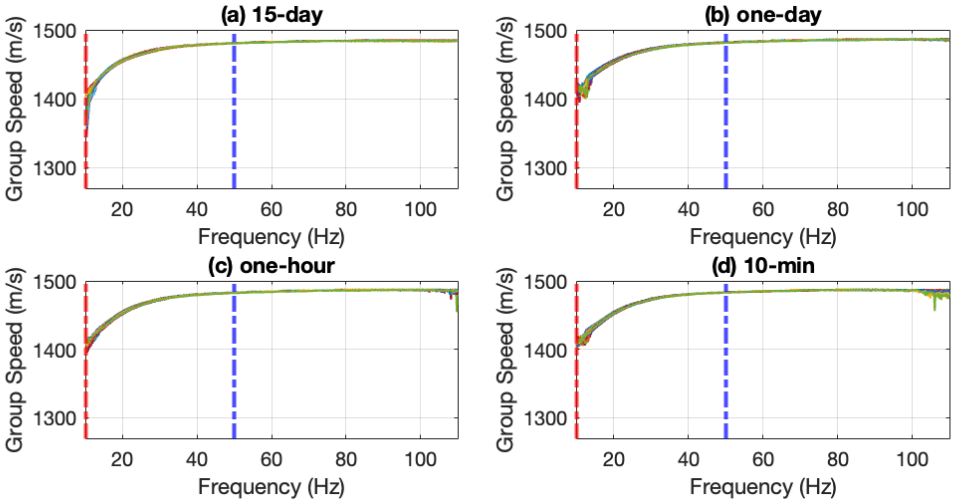

The Dispersion curves of mode #1. Note that below low-frequency threshold (red-dashed line) is the low-frequency region, beyond the mid-frequency threshold is the high-frequency region, and between thresholds is the mid-frequency region. Each panel represents different observation periods which are specified by corresponding titles.

Figure 25. Normal mode dispersion curves for mode #1 in four different observation periods

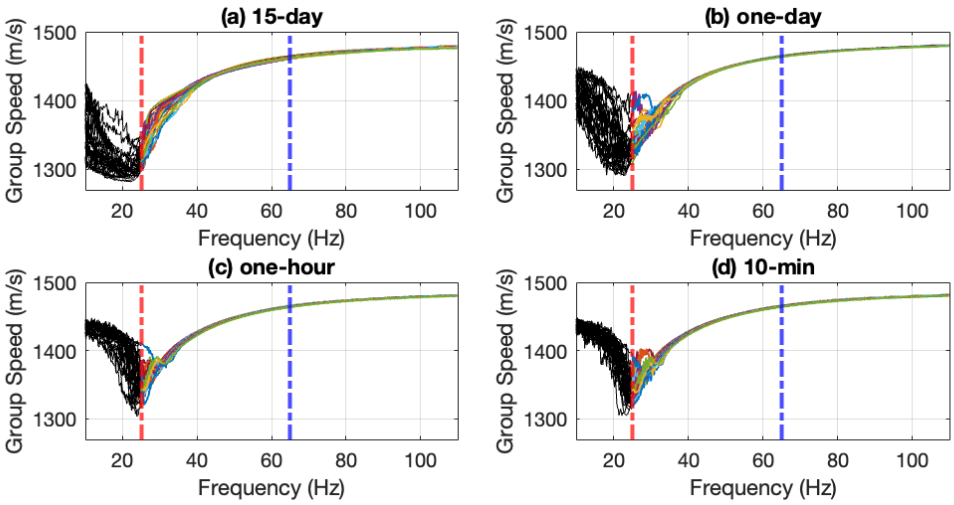

Same as Figure 25 but for mode #2.

Figure 26. Normal mode dispersion curves for mode #2 in four different observation periods

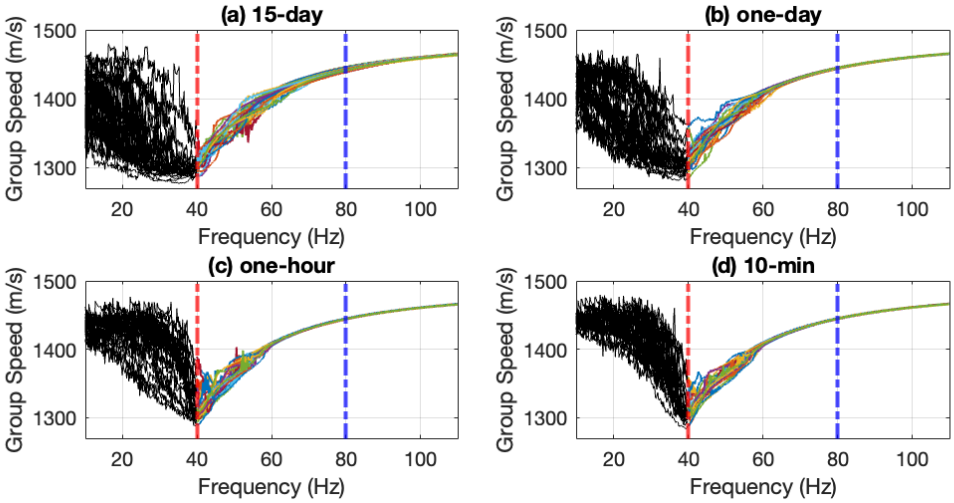

Same as Figure 26 but for mode #3.

Figure 27. Normal mode dispersion curves for mode #3 in four different observation periods

In the mid-frequency region shown in Figure 28, the dispersion curves start to be divergent, i.e., the standard deviations significantly increase. The divergence of the dispersion curves represents the inconsistency between 31 measurements and makes this frequency band less reliable. It should be noted Tan et al. [10] suggest that excluding the

region with higher uncertainty improves the geoacoustic inversion results. While comparing the results of dispersion curves, we exclude a portion of the frequency band in the mid-frequency region where the standard deviations are relatively high (Figure 28). Thus, the reliable frequency bands are a portion of the mid-frequency region where the uncertainty is relatively small, and the high-frequency region.

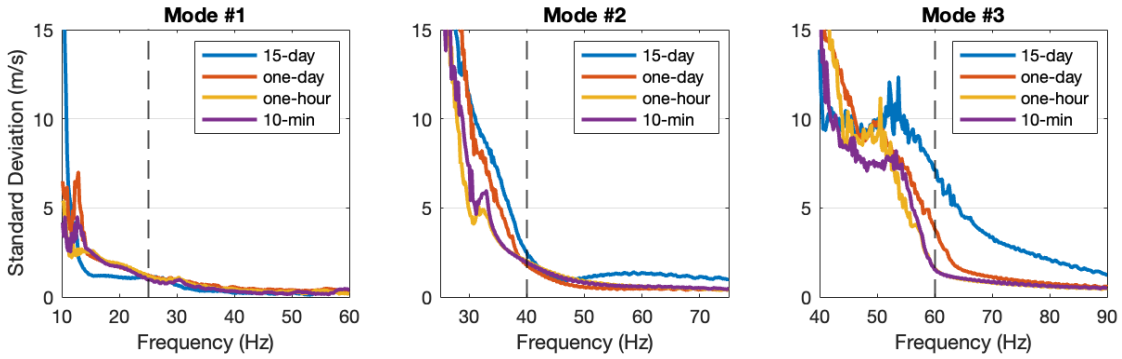

The standard deviation of 31 measurements in different averaging observation periods. The frequency band below the threshold (black-dashed line) is considered as high uncertainty.

Figure 28. Standard deviation of 31 measurements in mid-frequency region

The dispersion curves shown in Figure 29 are the averaged dispersion curves (red-solid line) with uncertainty area (red-shaded region). The uncertainty represents one standard deviation based on the dispersion curves from 31 NCCFs. The best-fitting dispersion curves (black-dashed line) were obtained by normal mode code KRAKEN [28] and geoacoustic model of the seabed shown in Table 3. The geoacoustic model is based on three layers, six acoustic parameters, and a sound speed profile. The three layers include water column, fluid sediment, and fluid half-space basement, and the corresponding six parameters are water depth D of the water column, sediment layer thickness H, sound speed c_s, c_b, and the ratio of density ρ_s, ρ_b of the sediment and basement. The parameters used in the geoacoustic model were found by solving the geoacoustic inversion problem in Tan et al. [10]. The sound speed profile used in the acoustic model is the sound speed averaged over 15 days which was measured close to HLA and shown in Figure 4 (a).

Table 3. Geoacoustic model. Adapted from [10].

Model Layers	Acoustic Parameters	Inversion Results
Water Column	Sound Speed Profile *SSP*	-
	Water Depth D	81 (m)
Fluid Sediment	Sound Speed c_s	1620 (m/s)
	Ratio of Density ρ_s	1.4
	Sediment Layer Thickness H	15 (m)
Fluid Half-space Basement	Sound Speed c_b	2050 (m/s)
	Ratio of Density ρ_b	2.35

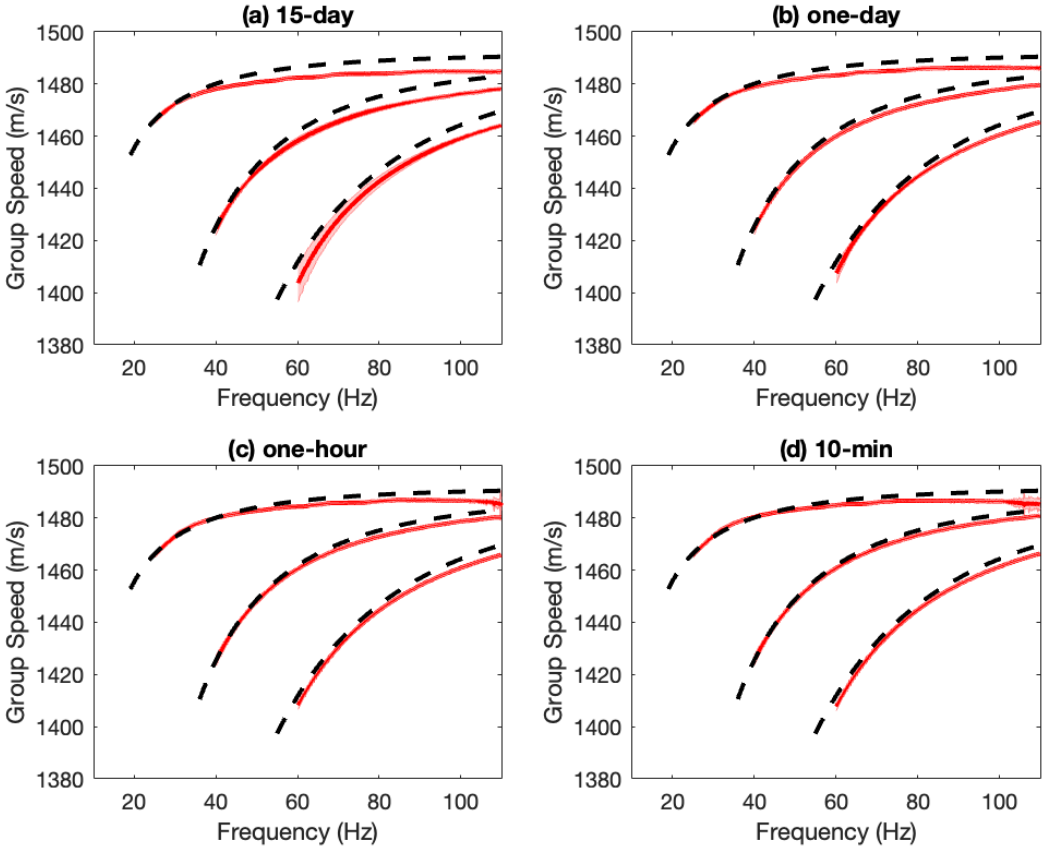

The KRAKEN best-fitting dispersion curves are shown by black-dashed line and empirical dispersion curves are shown by red line with red-shaded uncertainty. The uncertainty is the one standard deviation of 31 measurements. Each panel represents different observation periods, which are specified by corresponding titles.

Figure 29. Averaged normal mode dispersion curves of 15-day NCCFs

3. Difference Compared to the Best-fitting Curves

The difference between the empirical dispersion curves and the best-fitting curves gives the quantitative performance of four observation periods shown in Figure 30 and Figure 31. Note the frequency bands in each mode are different due to the exclusion of low-frequency and mid-frequency bands discussed in Subsection IV.B.2. The results of mode #1 and mode #2 are shown in Figure 30. Overall, the three short-time observation periods achieve a smaller difference than the one of the 15-day observation period. Also, the difference increases with frequency in both mode #1 and mode #2. A partial cause is that group speed always increases with frequency in dispersion curves and inevitably makes measurement error bigger. Another possible reason is that the way we design modal masks creates a systematical error.

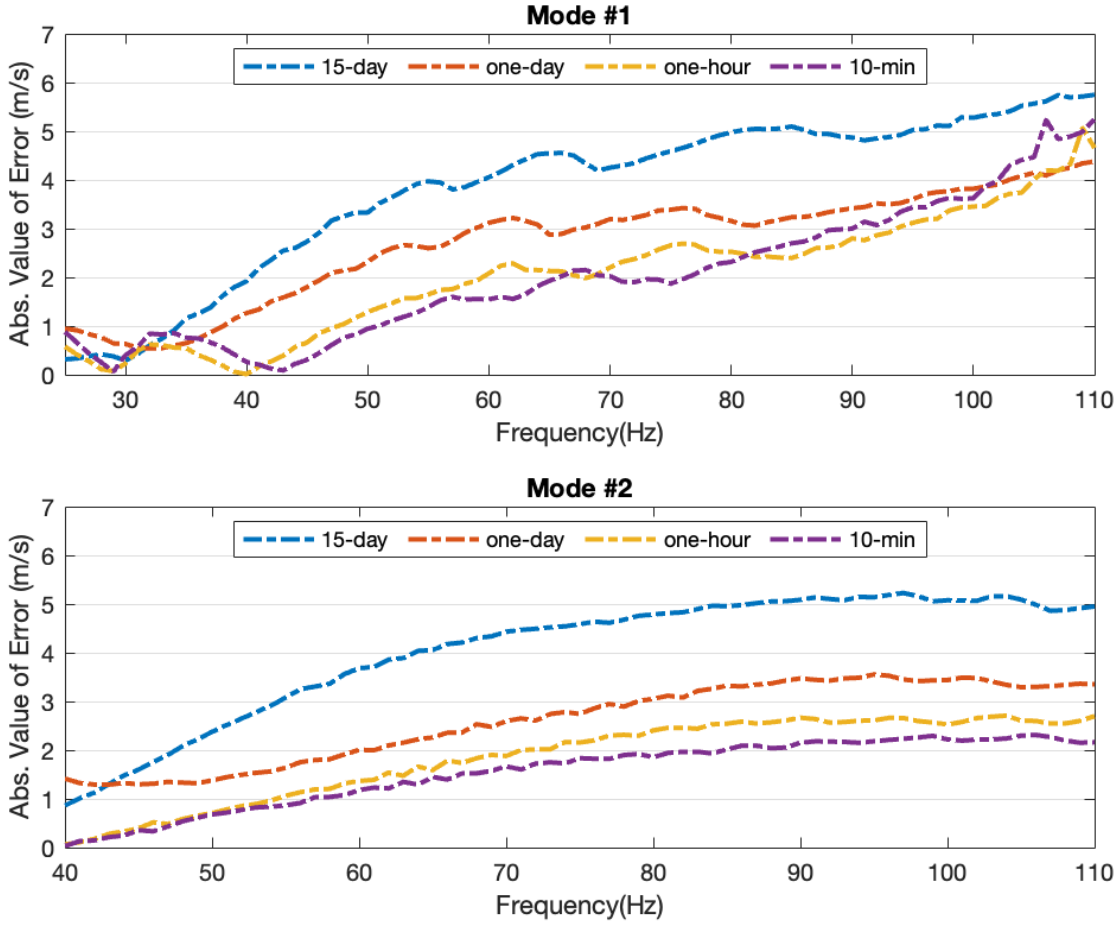

Figure 30. Difference between empirical dispersion curves of mode #1-2 and KRAKEN best-fitting curves

The result of mode #3 is shown in Figure 31. Unlike mode #1 and mode #2, the result of mode #3 shows the opposite trend in its lower frequency part (60-75 Hz band). Beyond 75 Hz, we see the same trend observed in mode #1 and mode #2. Overall, the differences among the three short-time observation periods are consistent and considerably smaller than the 15-day observation period.

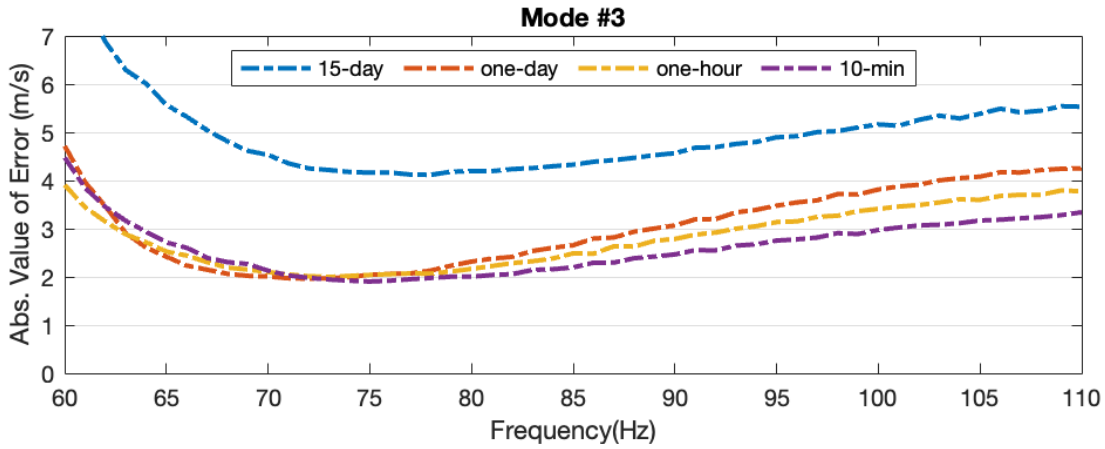

Figure 31. Difference between empirical dispersion curves of mode #3 and KRAKEN best-fitting curves

4. Summary and Discussion

In this section, the dispersion curves of normal modes are successfully retrieved from the EGFs of the four different observation periods. We exclude the unphysical and unreliable frequency band from the retrieved dispersion curves. By comparing with a well-established geoacoustic model, we conclude that the EGFs of the short-time observation periods can achieve smaller differences than ones of the long-time observation period. However, the systematical trends are evident in both modes. A possible reason is how we design modal masks is universal for all 31 measurements instead of customizing individual masks for each measurement. It should be noted that the geoacoustic model we compare with is imperfect. More detailed analysis can be achieved by conducting geoacoustic inversion based on the empirical dispersion curves in Figure 29.

THIS PAGE INTENTIONALLY LEFT BLANK

V. CONCLUSIONS

A. SUMMARY

Noise interferometry has been proven to be capable of passively characterizing an underwater environment. The usefulness of noise interferometry relies on the oceanographically relevant accuracy of the retrieval of normal mode dispersion curves. These acoustic parameters are retrieved from the noise cross-correlation functions (NCCFs) between two spatially separated hydrophones. A long averaging period is usually adopted to improve the quality of NCCFs provided that the ocean environment is stable throughout the averaging period. This condition cannot be fulfilled in a variable ocean environment where environmental information is highly desirable in military operations. Besides, the long-averaging period limits the applications of noise interferometry in urgent missions. This thesis has explored the possibility of rapidly estimating NCCFs for passively acoustic characterization of the ocean.

In Chapter III, three short-time N-NCCFs are selected based on their correlation with 15-day N-NCCFs. In Figure 12 and Figure 13, all three short-time N-NCCFs are shown to be as good as or better than the 15-day N-NCCFs. A possible drawback of using a short averaging period is useful NCCFs only emerge at either positive time delay (P-NCCFs) or negative time delay (N-NCCFs). The reason is the diffusivity of ambient noise requires a certain amount of averaging time to manifest. However, to acoustically characterizing a water column and seabed, we only require one side of NCCFs, i.e., either P-NCCFs or N-NCCFs, to retrieve empirical Green's functions (EGFs). This drawback only restricts the noise interferometry applications which rely on the reciprocity/nonreciprocity between P-NCCFs and N-NCCFs.

In Chapter IV, we build a judiciously-built procedure to apply the time-warping transform to the EGFs, then obtain acoustic dispersion curves of normal modes, respectively. The results in Figure 29 show the EGFs retrieved from the as short as 10-min NCCFs can be high-quality compared to the EGFs retrieved from the long-time NCCFs. Also, this procedure can be utilized to preliminarily assess the quality of NCCFs

automatically in future work without human intervention. There are two conclusions drawn in this chapter. First, Table 2 shows that using a short averaging period can preserve higher modal energy especially for mode #2 and mode #3. This suggests exploring the contribution of high-order modes obtained from NCCFs averaged over a short observation period. Second, in Section IV. B., we compare retrieved dispersion curves with the dispersion curves obtained by normal mode code KRAKEN and the previously established geoacoustic model. Given that EGFs are sufficiently accurate, the result in Figure 30 and Figure 31 indicates the EGFs with a short averaging observation period can achieve better accuracy of acoustic dispersion curves.

B. CONCLUSIONS AND FUTURE WORK

The NCCFs, which are averaged over a short and judiciously-chosen observation period, allows one to apply acoustic interferometry for surreptitious remote sensing in a rapidly changing acoustic environment. Eliminating the redundant averaging time improves the flexibility of characterizing the littoral ocean via noise interferometry, allowing more rapid estimates of geoacoustic and oceanographic parameters.

In future research, one can conduct geoacoustic inversions based on the dispersion curves retrieved from the selected short-time NCCFs in this study and corresponding measured sound speed profiles. By comparing the inversion results with other reliable geoacoustic models, more detail analysis of the performance of the shot-time NCCFs can be achieved. In addition, one can exploit the automated time-warping transform developed in this thesis to an abundance of NCCFs averaged over a consecutive short observation period throughout the available temporal span of the SW06 experiment. By doing an exhaustive search, one can determine the quality of NCCFs and then relate the corresponding oceanographic feature to those time slots with high-quality NCCFs.

LIST OF REFERENCES

[1] S. L. Kastner, "Is the Taiwan strait still a flash point? Rethinking the prospects for armed conflict between China and Taiwan," *International Security,* vol. 40, no. 3, pp. 54–92, 2015.

[2] R. D. Kaplan, "The South China Sea is the future of conflict," *Foreign Policy,* no. 188, p. 76, 2011.

[3] P. Roux, W. Kuperman, and N. Group, "Extracting coherent wave fronts from acoustic ambient noise in the ocean," *The Journal of the Acoustical Society of America,* vol. 116, no. 4, pp. 1995–2003, 2004.

[4] K. G. Sabra, P. Roux, A. M. Thode, G. L. D'Spain, W. Hodgkiss, and W. Kuperman, "Using ocean ambient noise for array self-localization and self-synchronization," *IEEE Journal of Oceanic Engineering,* vol. 30, no. 2, pp. 338–347, 2005.

[5] O. A. Godin, "Recovering the acoustic Green's function from ambient noise cross correlation in an inhomogeneous moving medium," *Physical Review Letters,* vol. 97, no. 5, p. 054301, 2006.

[6] O. A. Godin, "Cross-correlation function of acoustic fields generated by random high-frequency sources," *The Journal of the Acoustical Society of America,* vol. 128, no. 2, pp. 600–610, 2010.

[7] O. A. Godin, M. G. Brown, N. A. Zabotin, L. Y. Zabotina, and N. J. Williams, "Passive acoustic measurement of flow velocity in the Straits of Florida," *Geoscience Letters,* vol. 1, no. 1, p. 16, 2014.

[8] O. A. Godin, N. A. Zabotin, and V. V. Goncharov, "Ocean tomography with acoustic daylight," *Geophysical Research Letters,* vol. 37, no. 13, 2010.

[9] K. F. Woolfe, S. Lani, K. G. Sabra, and W. A. Kuperman, "Monitoring deep-ocean temperatures using acoustic ambient noise," *Geophysical Research Letters,* vol. 42, no. 8, pp. 2878–2884, 2015.

[10] T. W. Tan, "Application of acoustic noise interferometry to remote sensing of a coastal ocean," Ph.D. dissertation, Dept. of Phy. Monterey, CA; Naval Postgraduate School, 2019.

[11] R. M. Mcmullin, "Application of time reversal to passive acoustic characterization of the ocean," M.S. thesis, Dept. of Phy., Monterey, CA; Naval Postgraduate School, 2019.

[12] M. G. Brown, O. A. Godin, N. J. Williams, N. A. Zabotin, L. Zabotina, and G. J. Banker, "Acoustic Green's function extraction from ambient noise in a coastal ocean environment," *Geophysical Research Letters,* vol. 41, no. 15, pp. 5555–5562, 2014.

[13] O. A. Godin, B. Katsnelson, and T. W. Tan, "Normal mode dispersion and time warping in the coastal ocean," *The Journal of Acoustical Society of America,* vol. 146, no. 3, pp. EL205-EL211, 2019.

[14] R. G. Baraniuk and D. L. Jones, "Unitary equivalence: A new twist on signal processing," *IEEE Transactions on Signal Processing,* vol. 43, no. 10, pp. 2269–2282, 1995.

[15] G. Le Touzé, B. Nicolas, J. I. Mars, and J.-L. Lacoume, "Matched representations and filters for guided waves," *IEEE Transactions on Signal Processing,* vol. 57, no. 5, pp. 1783–1795, 2009.

[16] T. Tan, O. A. Godin, A. Lefebvre, W. Beaute, B. G. Katsnelson, and M. Yarina, "Characterizing the seabed by using noise interferometry and time warping," in *Proceedings of Meetings on Acoustics 176ASA*, 2018, vol. 35, no. 1: ASA, p. 070001.

[17] J. Bonnel, A. Thode, D. Wright, and R. Chapman, "Nonlinear time-warping made simple: A step-by-step tutorial on underwater acoustic modal separation with a single hydrophone," *The Journal of the Acoustical Society of America,* vol. 147, no. 3, pp. 1897–1926, 2020.

[18] J. Bonnel and N. R. Chapman, "Geoacoustic inversion in a dispersive waveguide using warping operators," *The Journal of the Acoustical Society of America,* vol. 130, no. 2, pp. EL101-EL107, 2011.

[19] T. W. Tan, O. A. Godin, M. G. Brown, and N. A. Zabotin, "Characterizing the seabed in the Straits of Florida by using acoustic noise interferometry and time warping," *The Journal of the Acoustical Society of America,* vol. 146, no. 4, pp. 2321–2334, 2019.

[20] J. Bonnel, S. E. Dosso, and N. Ross Chapman, "Bayesian geoacoustic inversion of single hydrophone light bulb data using warping dispersion analysis," *The Journal of the Acoustical Society of America,* vol. 134, no. 1, pp. 120–130, 2013.

[21] J. Zeng, N. R. Chapman, and J. Bonnel, "Inversion of seabed attenuation using time-warping of close range data," *The Journal of the Acoustical Society of America,* vol. 134, no. 5, pp. EL394-EL399, 2013.

[22] R. Duan, N. Ross Chapman, K. Yang, and Y. Ma, "Sequential inversion of modal data for sound attenuation in sediment at the New Jersey Shelf," *The Journal of the Acoustical Society of America,* vol. 139, no. 1, pp. 70–84, 2016.

[23] A. E. Newhall *et al.*, "Acoustic and oceanographic observations and configuration information for the WHOI moorings from the SW06 experiment," Woods Hole Oceanographic Institution, MA, 2007.

[24] J.-X. Qin, B. Katsnelson, O. Godin, and Z.-L. Li, "Geoacoustic inversion using time reversal of ocean noise," *Chinese Physics Letters,* vol. 34, no. 9, p. 094301, 2017.

[25] J. Benesty, J. Chen, Y. Huang, and I. Cohen, "Pearson correlation coefficient," in *Noise Reduction in Speech Processing*: Springer, 2009, ch 1, pp. 1–4.

[26] D. F. Williamson, R. A. Parker, and J. S. Kendrick, "The box plot: a simple visual method to interpret data," *Annals of Internal Medicine,* vol. 110, no. 11, pp. 916–921, 1989.

[27] F. Auger and P. Flandrin, "Improving the readability of time-frequency and time-scale representations by the reassignment method," *IEEE Transactions on signal processing,* vol. 43, no. 5, pp. 1068–1089, 1995.

[28] M. B. Porter, *The KRAKEN Normal Mode Program*, Washington, DC, Naval Research Lab, 1992.

THIS PAGE INTENTIONALLY LEFT BLANK

INITIAL DISTRIBUTION LIST

1. Defense Technical Information Center
   Ft. Belvoir, Virginia

2. Dudley Knox Library
   Naval Postgraduate School
   Monterey, California